Assessing acetone for the GISS ModelE2.1 Earth system model

Alexandra Rivera[1], Kostas Tsigaridis[2,3], Gregory Faluvegi[2,3], Drew Shindell[4]

[1]Pratt School of Engineering, Duke University, Durham, NC, 27708, USA
[2]Center for Climate Systems Research, Columbia University, 2880 Broadway, New York, NY, 10025, USA
[3]NASA Goddard Institute for Space Studies, 2880 Broadway, New York, NY, 10025, USA
[4]Nicholas School of the Environment, Duke University, Durham, NC, 27708, USA

Correspondence to: Kostas Tsigaridis (kostas.tsigaridis@columbia.edu)

Abstract. Acetone is an abundant volatile organic compound in the atmosphere with important influence on ozone and oxidation capacity. Direct sources include anthropogenic, terrestrial vegetation, oceanic, and biomass burning emissions. Acetone is also produced chemically from other volatile organic compounds. Sinks include deposition onto the land and ocean surfaces, as well as chemical loss. Acetone's lifetime is long enough to allow transport and reactions with other compounds remote from its sources. The latest NASA Goddard Institute for Space Studies (GISS) Earth System Model, ModelE2.1, simulates a variety of Earth system interactions. Previously, acetone had a very simplistic representation in the ModelE chemical scheme. This study assesses a more sophisticated acetone scheme, in which acetone is a full 3-dimensional tracer, with explicit sources, sinks and atmospheric transport. We evaluate the new global acetone budget in the context of past literature. Anthropogenic emissions, vegetation emissions, biomass burning, and deposition representations agree well with previous studies. Chemistry and the ocean contribute to both sources and sinks of acetone, with their net values agreeing with the literature, although their individual source and sink terms appear to be overestimated for chemistry and underestimated for ocean fluxes. We find the production of acetone from precursor hydrocarbon oxidation has strong leverage on the overall chemical source, indicating the importance of accurate molar yields for this source. Spatial distributions reveal that ocean uptake of acetone is strongest in northern latitudes, while production is mainly in mid-southern latitudes. The seasonality of acetone-related processes was also studied in conjunction with field measurements around the world. These comparisons show promising agreement, but have shortcomings at urban locations, since the model's resolution is too coarse to capture behavior in high-emission areas. Overall, our analysis of the acetone budget aids the development of this tracer in the GISS ModelE2.1, a crucial step to understanding the role of acetone in the atmosphere.

1 Introduction

Acetone (C_3H_6O) is an abundant oxygenated volatile organic compound (VOC) that has important connections to ozone and the atmosphere's self-cleansing oxidation capacity (Read et al., 2012). Acetone's dynamic presence in Earth's atmosphere can be described through sources, sinks, and mechanisms of transport. Extensive literature has discussed the nature of these sources and sinks, and some are more well-constrained than others.

Primary sources of acetone in the atmosphere include anthropogenic, terrestrial vegetation, and biomass burning emissions. Past literature has found the fluxes of these sources to range between 1-2 Tg yr^{-1}, 30-45 Tg yr^{-1}, 2.5-4.5 Tg yr^{-1}, respectively (Beale et al., 2013; Brewer et al., 2017; Elias et al., 2011; Fischer et al., 2012; Folberth et al., 2006; Jacob et al., 2002; Singh et al., 2000; Wang et al., 2020). Chemical production from other VOCs with 3 or more carbon atoms, each with their own molar yields, is another source of acetone in the atmosphere (Brewer et al., 2017; Fischbeck et al., 2017; Hu et al., 2013; Jacob et al., 2002; Singh et al., 2000; Weimer et al., 2017).

Sinks of acetone include wet and dry deposition onto the land surface, as well as chemical loss. Wet deposition occurs within and below clouds due to the solubility of acetone, and depends on its Henry's Law coefficient (Benkelberg et al., 1995). Dry deposition occurs on the land surface. Chemical loss of acetone forms radicals through photolysis. Past literature has estimated the acetone sinks to be 10-30% dry deposition, and 40-85% chemical loss (Arnold et al., 2005; Elias et al., 2011; Fischer et al., 2012; Khan et al., 2015; Singh et al., 1994). The estimated fluxes are 10-16 Tg yr^{-1} and 45-60 Tg yr^{-1} for total deposition and chemical loss, respectively (Arnold et al., 2005; Brewer et al., 2017; Dufour et al., 2016; Elias et al., 2011; Fischer et al., 2012; Jacob et al., 2002; Khan et al., 2015; Marandino et al., 2005; Singh et al., 2000; Wang et al., 2020).

The ocean surface is a bidirectional flux that provides both a source and a sink for acetone. Ocean surface conditions such as wind speed, sea surface temperature, and seawater concentration of acetone can influence the direction and magnitude of ocean-acetone exchange (Wang et al., 2020). Previous literature estimates an oceanic source flux of 25−50 Tg yr^{-1} and oceanic uptake flux of 35−60 Tg yr^{-1}. However, there is little consensus in the literature on whether the ocean serves as a net source or sink of acetone, with some studies indicating a net oceanic source (Beale et al., 2013; Jacob et al., 2002; Wang et al., 2020), and other studies indicating a net oceanic sink (Brewer et al., 2017; Elias et al., 2011; Fischer et al., 2012; Wang et al., 2020).

In addition to a global annual mean atmospheric budget, previous studies have reported the seasonality of acetone-related processes. Past studies have compared monthly estimates of acetone mixing ratios to field measurements of European sites from Solberg et al. (1996) (Arnold et al., 2005; Elias et al., 2011; Jacob et al., 2002). Comparisons with these European sites have emphasized the seasonal variability of acetone emissions, as nearly all sites portray a summer maximum and winter minimum of acetone abundance. Vegetation emissions from June to September, along with chemical sources, have an especially strong contribution to this seasonality. The winter minimum of acetone is aided by an ocean sink at coastal sites (Jacob et al., 2002).

Other studies have described spatial distributions and seasonal dependence of ocean fluxes of acetone (Fischer et al., 2012; Wang et al., 2020). A model by Fischer et al. (2012) proposed a net ocean sink of 2 Tg yr^{-1} and characterized ocean uptake of acetone as strongest in northern latitudes year-round and in the high southern latitudes during the winter. An oceanic acetone source was dominant in the tropical regions, with an exception off the Western coasts of Central America and Central Africa (Fischer et al., 2012). A model by Wang et al. (2020) that varied surface seawater acetone concentration through a machine learning approach also proposed a net ocean sink year-round. This net sink was strongest in December-February, and weakest in March-May.

The vertical distribution of acetone has been modelled between the seasons of May-October and November-April in the surface and troposphere (Fischer et al., 2012). Acetone concentrations are generally higher in the lower altitudes due to proximity to surface emissions. Surface-level acetone has been measured over a variety of terrestrial and oceanic sites around the world (de Gouw et al., 2004; Dolgorouky et al., 2012; Galbally et al., 2007; Guérette et al., 2019; Hu et al., 2013; Huang et al., 2020; Langford et al., 2010; Lewis et al., 2005; Li et al., 2019; Read et al., 2012; Schade and Goldstein, 2006; Singh et al., 2003; Solberg et al., 1996; Warneke and de Gouw, 2001; Yoshino et al., 2012; Yuan et al., 2013), and in some cases, these measurements were taken over a variety of months to provide a sense of seasonality (Dolgorouky et al., 2012; Hu et al., 2013; Read et al., 2012; Schade and Goldstein, 2006; Solberg et al., 1996). Additionally, vertical distributions of acetone have been measured through NASA's Atmospheric Tomography Mission (ATom) campaigns (Thompson et al., 2022). The ATom-1, ATom-2, ATom-3, and ATom-4 campaigns took place during July-August 2016, January-February 2017, September-October 2017, and April-May 2018,

respectively. Each campaign provided mixing ratios for a variety of VOCs in profiles from the marine boundary layer up to the upper troposphere/lower stratosphere (Apel et al., 2021).

The NASA Goddard Institute for Space Studies (GISS) ModelE2.1 Earth System Model (Kelley et al., 2020) has the capability of simulating a variety of Earth system interactions, is used both to interpret and predict past and future climate, and routinely participates in the Climate Model Intercomparison Projects (CMIP) and Intergovernmental Panel for Climate Change (IPCC) reports. Here we used and enhanced this model by adding acetone as an independent chemical tracer (Kelley et al., 2020). Previously, acetone had a very simplistic representation in the model's chemical scheme (Shindell et al., 2003), in which acetone's spatial variation was parameterized based on the difference of the model's zonal mean distribution of isoprene and that tracer's three-dimensional distribution. Acetone's lifetime is long enough to be transported remote from sources, but not long enough to become uniformly mixed, and therefore its simulated distribution should benefit from a more realistic implementation. We developed a greatly improved acetone tracer scheme by making prognostic calculations of the 3-dimensional distribution of acetone as a function of time. We evaluated its atmospheric burden and lifetime as well as source/sink fluxes (anthropogenic emissions, vegetation emissions, biomass burning, deposition, ocean, and chemistry) against other models and its concentration against field measurements. This work aims to provide a holistic assessment of the abundance of acetone in the atmosphere.

2 Methodology

Here we implement acetone in the GISS ModelE2.1 based on the literature rather than developing a new parameterization. Our 'Baseline' simulation is a climatological mean with year 2000 conditions, chosen to be relatively modern without precluding comparison with models in older literature. The 1996-2004 mean of prescribed emissions from Hoesly et al. (2018) were used, along with the 1996-2005 mean sea surface temperature and sea ice cover as described in Kelley et al. (2020). Acetone simulations use full chemistry and not archived OH fields. An additional simulation, 'Nudged_ATom', was conducted to compare more directly with ATom field measurements. This simulation employed nudged winds (from MERRA2) (Gelaro et al., 2017) and ocean surface conditions and trace gas and aerosol emissions changing with time during 2016-2018.

2.1 Sources

2.1.1 Anthropogenic emissions

Anthropogenic emissions were prescribed using the 1996-2004 averages of the Community Emissions Data System (CEDS) emissions from Hoesly et al. (2018) as prepared for the GISS contributions to the Coupled Model Intercomparison Project, Phase 6 (CMIP6) (Kelley et al., 2020). These include sources from agriculture, the energy sector, the industrial sector, residential/commercial/other, international shipping, solvents production and application, the transportation sector, and waste. In line with past studies, we base acetone emissions on that of ketones. VOC23-ketones emissions from Hoesly et al. (2018) were scaled down by a ratio of acetone molecular weight to an average ketone molecular weight (58.08 g mol^{-1}/75.3 g mol^{-1}). Maintaining the resulting spatial and temporal pattern of emissions, the magnitudes were then tuned to be close to that of Fischer et al. (2012), resulting in a total of about 1 Tg yr^{-1}. This resulted in roughly 36.5% of CEDS VOC23-ketones used as acetone emissions. Lacking an accurate way to obtain acetone aircraft emissions from the bulk VOCs available in the emission inventory, we have neglected that sector in the simulations.

2.1.2 Terrestrial vegetation emissions

Emissions from land vegetation were derived from the Model Emissions of Gases and Aerosols from Nature (MEGAN), version 2.1 (Guenther et al., 2012), a new contribution to the ModelE. Emission response algorithms in the MEGAN2.1 model are derived from input leaf area indices, solar radiation, temperature, moisture, CO_2 concentrations, and plant functional types and composition of species (Guenther et al., 2012). The acetone vegetation emissions in the Baseline simulation in GISS ModelE2.1 are calculated to equal 36.1 Tg yr^{-1}.

2.1.3 Biomass burning emissions

Acetone emissions were prescribed from a 1996-2004 average of the NMVOC-C3H6 species from version 2.1 of the biomass burning dataset of van Marle et al. (2017), used by CMIP6. The acetone mass flux from biomass burning in the Baseline simulation was 1.59 Tg yr^{-1}.

Figure 1 shows the biomass burning emission rate chosen for this study, and how it lies within the range of substantial interannual variability. During the 20-year period shown, emissions averaged 1.463 Tg yr^{-1}, with a standard deviation of 0.402, and a spike in the earlier years of emissions over 2.75 Tg yr^{-1} is also observed (Figure 1). On top of any differences across emission inventories, the years considered when reporting emissions may be the reason for variability between models (e.g. 2.40 – 2.80 Tg yr^{-1} from the 2006 GFED-v2 emission inventory in Elias et al. (2011) and Fischer et al. (2012), compared to 3.22 Tg yr^{-1} from 1997-2001 in Folberth et al. (2006)).

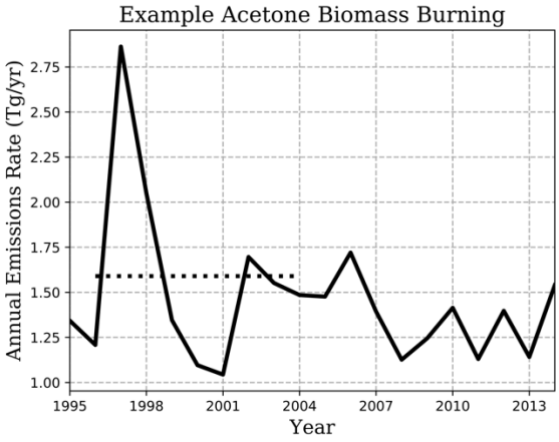

Figure 1. Illustration of interannual variability of NMVOC-C3H6 biomass burning emissions of van Marle et al. (2017) (solid line), used as acetone emissions in our simulation. Climatological-emissions simulations use the 1996-2004 mean (dotted line), though emissions vary by month.

2.2 Sinks

2.2.1 Deposition

Both dry and wet deposition of acetone were included in the model, although dry deposition was, on average, 91% of total deposition. The wet deposition scheme is given by Koch et al. (1999). Acetone and other species are transported within and below clouds, and soluble gases are deposited depending on the conditions of the grid box they are in and a Henry's Law Coefficient (Shindell et al., 2001). The Henry's Law Coefficient for acetone used in the GISS ModelE2.1 is 27 mol L^{-1} atm^{-1}, with a Henry temperature dependence of acetone of 5300 J mol^{-1} (Benkelberg et al., 1995; Zhou and Mopper, 1990). The dry deposition scheme

uses resistance-in-series calculations, global seasonal vegetation data (Chin et al., 1996; Shindell et al., 2001; Wesely and Hicks, 1977), and a reactivity factor of f_0=0.1. This resulted in an acetone deposition rate in the Baseline simulation of 22.2 Tg yr^{-1}.

2.3 Chemistry

The GISS ModelE2.1 Baseline simulation estimates a net chemistry change of -20.6 Tg yr^{-1}. The components can be broken up into sources and sinks as follows.

2.3.1 Chemical sources

The Baseline simulation estimates chemical production to be 33.3 Tg yr^{-1}. The acetone chemical scheme includes two production reactions:

$$Paraffin + OH \rightarrow 0.35\ Acetone \quad (1)$$

$$Terpenes + \{OH, O_3\} \rightarrow 0.12\ Acetone \quad (2)$$

In the first reaction, acetone is produced by paraffin, a proxy tracer for paraffinic (saturated) carbon, and OH (Eq. 1). The molar yield of acetone from paraffin was found to be a strong leverage to the overall chemical source (see Section 3.5). A rate coefficient of 8.1E-13 cm^3 $molecule^{-1}$ s^{-1} was used (Shindell et al., 2003). Previous literature has suggested an acetone yield on a molecular scale of 0.72 (Fischbeck et al., 2017; Jacob et al., 2002; Weimer et al., 2017). Initial tests using a yield of 0.72 resulted in an overestimated chemistry source, leading us to re-evaluate this yield for the specific mixture of VOCs represented in the GISS ModelE2.1.

Our model's anthropogenic emissions of paraffin is based on an aggregation of selected VOC groups. Based on year 2019 emissions of the O'Rourke et al. (2021) dataset, we emit paraffin that is about 11% propane by mole, 22% butane and 21% pentane. Multiplying these by each VOC's acetone molar yield (0.73, 0.95, 0.63, respectively), we estimate that 42% of paraffin from anthropogenic sources becomes acetone in our model. Paraffin biomass burning emissions, estimated from year 2020 of SSP3_70 emissions (Riahi et al., 2017; Fujimori et al., 2017) contain mole fractions for propane of 9% and higher alkanes of 23%, and when multiplied by acetone molar yields of 0.73 and 0.79, respectively, suggest that about 25% of paraffin from biomass burning sources becomes acetone in our model. The molar yields used in these calculations were derived with suggestions from the literature (Fischbeck et al., 2017; Jacob et al., 2002; Weimer et al., 2017). Refer to the manuscript supplement for a more detailed breakdown. Overall, an average of the 42% anthropogenic paraffin and 25% biomass burning paraffin was used to conclude that approximately 35% of paraffin from emissions becomes acetone, leading to our refinement of the molar yield in Eq. (1) to 0.35.

Additionally, reactions between terpenes and {OH, O_3} were implemented with an acetone yield of 0.12 (Hu et al., 2013; Jacob et al., 2002) (Eq. 2). The rates for these reactions are 2.51E-11*exp(444/T) cm^3 $molecule^{-1}$ s^{-1} for the OH reaction and 1.40E-14*exp(-732/T) cm^3 $molecule^{-1}$ s^{-1} for the O_3 reaction, and these coefficients are enhanced from the standard α-pinene one to consider the reactivity variability across mono- and higher terpenes (Tsigaridis and Kanakidou, 2003).

2.3.2 Chemical sinks

The chemical sink of acetone in the Baseline simulation is estimated to be 53.8 Tg yr^{-1}. The sinks of acetone include oxidation by OH and Cl radicals, and photolysis:

$$Acetone + OH \rightarrow H_2O + CH_3C(O)CH_2\ (assumed\ to\ decompose\ to\ HCHO) \quad (3)$$

$$Acetone + Cl \rightarrow HCl + CH_3C(O)CH_2\ (assumed\ to\ decompose\ to\ HCHO) \quad (4)$$

$$Acetone + h\nu \rightarrow CH_3CO + CH_3 \quad (5)$$

$$Acetone + h\nu \rightarrow CH_3 + CH_3 + CO \quad (6)$$

The first and second acetone destruction reactions above have rates of 1.33E-13 + 3.82E-11*exp(-2000/T) cm^3 $molecule^{-1}$ s^{-1} and 7.70E-11*exp(-1000/T) cm^3 $molecule^{-1}$ s^{-1}, respectively (Sander et al., 2011) (Eq. 3, 4). Previously, acetone photolysis (which only affected production of radicals and not acetone itself) did not utilize the model's photolysis scheme but was parameterized solely as a function of orbital geometry and atmospheric pressure. In the model updates, photolysis now consists of two separate reactions, where acetone forms either CH_3CO + CH_3 radicals or two CH_3 radicals and CO (Eq. 5, 6). Reaction 5 is pressure-dependent, while reaction 6 is temperature-dependent. The spectroscopic data used for acetone photolysis is from JPL 2010 (Sander et al., 2011) and mapped onto Fast-J version 6.8d's wavelength intervals (Neu et al., 2007). The quantum yields are pressure and temperature dependent and thus vary with altitude and location. For example, in a standard atmosphere the ratio of the yield of CO to CH_3CO decreases from 0.28 at the surface to 0.18 at 4 km altitude.

2.4 Ocean

Bidirectional fluxes of acetone are calculated over ocean based on the "two-phase" model of molecular gas exchange at the air-sea interface of Liss & Slater (1974), as it is described in Johnson (2010). The fluxes are a function of simulated surface temperature and near-surface wind speed but independent of salinity. Henry's Law constants and temperature dependence of solubility for acetone are from Sander (1999). The atmospheric source from ocean water and sink from the atmosphere are calculated assuming a constant concentration of acetone in water (of 15 nM), the lower boundary layer atmospheric concentration, and the total transfer velocity (a combination of water-side and air-side transfer velocities). The constant concentration of 15 nM follows the implementation by Fischer et al. (2012) in the GEOS-CHEM model, who looked at observations and did not find a strong reasoning to make the concentration vary seasonally or spatially. The GISS ModelE2.1 Baseline simulation calculates the ocean to be a net source of acetone, producing 3.94 Tg yr^{-1}.

2.5 Sensitivity studies

Sensitivity studies were conducted to determine the influence of key parameters on the acetone budget and its global distribution (summarized in Table 1). Specifically, we were interested in seeing how much leverage a given parameter afforded the model by way of an artificial perturbation. Sensitivity studies for chemistry modify the sources of acetone. The Chem_Cl0 and Chem_Terp0 simulations provide no formation of acetone from chlorine or terpenes, respectively. The importance of paraffin is explored by halving its yield of acetone to 17.5% in the Chem_Par0.5 simulation, and by doubling its yield of acetone to 70% in the Chem_Par2.0 simulation. As vegetation was the most prominent source, the Veg_0.7 simulation observes its reduction by decreasing the MEGAN production of acetone by 30%. The Ocn_2.0 simulation aims to explore the impact of ocean acetone concentration by doubling it from 15 nM to 30 nM globally. The Dep_$f_0$0 simulation tested dropping the reactivity factor for dry deposition from 0.1 to zero. Finally, given the high interannual variability of biomass burning emissions, the BB_2.0 simulation explores the impact of doubling those emissions.

Table 1. Sensitivity studies conducted to observe the leverage a specific parameter afforded the model. Simulation names, as well as the parameter they target and a description, are included.

GISS ModelE2.1 Sensitivity Simulation	Sensitivity Parameter	Description

Chem_Cl0	Chemistry Source	Acetone + Chlorine reaction rate = 0
Chem_Terp0	Chemistry Source	No reaction for production of acetone from terpenes
Chem_Par0.5	Chemistry Source	Half the yield of acetone from paraffin (17.5%)
Chem_Par2.0	Chemistry Source	Double the yield of acetone from paraffin (70%)
Veg_0.7	Vegetation	0.7 factor of acetone from MEGAN
Ocn_2.0	Ocean	Ocean acetone concentration from 15nM to 30nM
Dep_$f_0$0	Dry Deposition	f_0 changed from 0.1 to 0
BB_2.0	Biomass Burning	Double biomass burning emissions

3 Results and model evaluation

3.1 Global acetone budget and burden

A global acetone budget table was compiled to place our estimates in context with past global modeling studies (Table 2) (Arnold et al., 2005; Beale et al., 2013; Brewer et al., 2017; Dufour et al., 2016; Elias et al., 2011; Fischer et al., 2012; Folberth et al., 2006; Guenther et al., 2012; Jacob et al., 2002; Khan et al., 2015; Marandino et al., 2005; Singh et al., 2000, 2004; Wang et al., 2020). The values of the individual fluxes in our model (global deposition, biomass burning, anthropogenic emissions, vegetation emissions, ocean net/source/sink, and chemistry net/source/sink) were mentioned previously.

Table 2. Global acetone budget table comparing burden, flux and lifetime estimates of acetone from the Baseline model to thirteen previous studies.

	This Study – Baseline [2021]	***Wang et al.* [2020]** [a]	***Wang et al.* [2020]** [b]	***Brewer et al.* [2017]**	***Fischer et al.* [2012]**	***Elias et al.* [2011]**	***Jacob et al.* [2002]**	**Other Estimates [2000-2016]** [e]
Burden (Tg)	2.93	3.50	3.80	5.57	5.60	7.20	3.80	3.50 – 4.20
Global Deposition (Tg yr^{-1})	-22.2	-25.2	-12.4	-12.4	-12.0	-19.0	-9.00	-26.0 – -6.0
Biomass Burning (Tg yr^{-1})	1.59	4.00	2.40	2.60	2.80	2.40	4.50	3.22 – 9.0
Anthro Emissions (Tg yr^{-1})	1.00	0.50	3.40	3.60	0.73	1.60	1.10	1.02 – 2.0
Vegetation Emissions (Tg yr^{-1})	36.1	39.8	32.2	37.1	32.0	76.0	35.0	15 – 56
Net Ocean (Tg yr^{-1})	3.94	-8.10	1.30	-7.50	-2.0	-8.0	13.0	4.00
Ocean Source (Tg yr^{-1})	15.2	33.4	45.7	51.8	80.0	20.0	27.0	20.0
Ocean Sink (Tg yr^{-1})	-11.3	-41.5	-44.4	-59.2	-82.0	-28.0	-14.0	-62.0
Net Chemistry (Tg yr^{-1})	-20.5	-11.1	-26.1	-22.5	-21.0	-53.0	-45.0	-33.0 – -5.50
Chem Source (Tg yr^{-1})	33.3	38.5	26.1	24.1	31.0	27.0	28.0	15.5 – 55.6
Chem Sink (Tg yr^{-1})	-53.8	-49.6	-52.2	-46.6	-52.0	-80.0	-73.0	-61.1 – -33.4
Chemical Lifetime (days) [c]	19.9	25.8	26.6	43.6	39.3	32.9	19.0	20.9 – 35.6

Lifetime (days) [d]	12.3	11.0	12.7	17.2	14.0	21.0	14.5	12.8 – 35

[a] CAM-Chem Model (Wang et al., 2020)
[b] GEOS-Chem Model (Wang et al., 2020)
[c] Chemical Lifetime = Burden/Chemical Sink
[d] Total Atmospheric Lifetime = Burden/Total Sink
[e] *Singh et al.* [2000, 2004], *Arnold et al.* [2005], *Folberth et al.* [2006], *Marandino et al.* [2006], *Guenther et al.* [2012], *Beale et al.* [2013], *Khan et al.* [2015], *Dufour et al.* [2016].

Atmospheric burden describes the total amount of acetone that is in the atmosphere. The GISS ModelE2.1 Baseline simulation estimates the burden to be 2.93 Tg. Additionally, chemical lifetime and atmospheric lifetime can be derived from burden. The chemical lifetime of acetone is calculated as the burden divided by the chemical sink, whereas total lifetime is the burden divided by all sinks. The chemical and total atmospheric lifetimes for the Baseline simulation are calculated to be 19.9 and 12.3 days, respectively. These values are also placed in the context of previous literature in Table 2.

The GISS ModelE2.1 Baseline acetone budget is further compared to previous model studies in Figure 2. The calculated fluxes in our Baseline simulation that are less than one standard deviation away from the literature mean include anthropogenic and vegetation emissions, net ocean, net chemistry, chemical production, and chemical destruction (Figure S1). Biomass burning in GISS ModelE2.1 appears as an outlier when compared against 9 previous model studies but can be attributed to the high interannual variability with emissions (as discussed in Section 2.1.3). The value of acetone deposition is on the high (more negative) end in GISS ModelE2.1 relative to 11 previous studies. This might be partially attributed to differences in deposition parametrization across models, as explored by our sensitivity study on dry deposition presented in section 3.5.2. The values for oceanic acetone sources and losses are smaller (in absolute values) than the mean from 7 previous model studies. Nevertheless, the net ocean flux matches the literature well. Lastly, the total atmospheric burden and lifetime calculated by GISS ModelE2.1 are lower than the previous papers, an expected consequence of the higher removal by deposition. The chemical lifetime is also calculated to be at the low end of published literature. As the burden is a function of many different atmospheric parameters, however, it was not the goal to corroborate our estimates with the literature as much as it was for each of the fluxes.

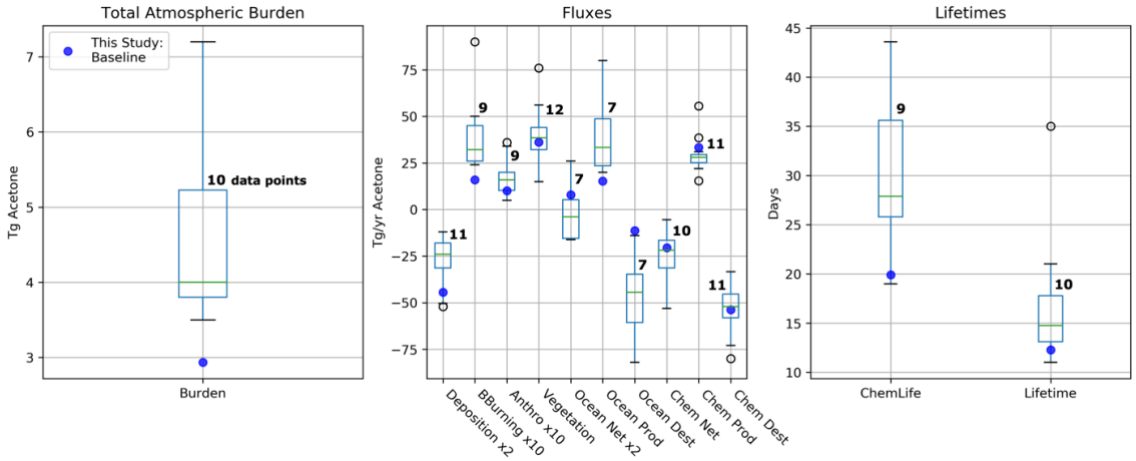

Figure 2. Total atmospheric burden, fluxes, and lifetimes of acetone from the literature values in Table 2 (shown in boxes and whiskers with outliers as open circles), and values from GISS ModelE2.1 (shown as solid circles). The number of models used to create each box and whisker plot are labelled. Note that deposition and ocean net fluxes were multiplied by 2 and biomass burning and anthropogenic emissions were multiplied by 10 for a better visualization of the distribution.

3.2 Spatial distribution of acetone

The global distribution of acetone at the surface is given in Figure 3. It is evident that acetone mixing ratios are largest over the continents, where anthropogenic, vegetation, and other terrestrial sources are located. Over the ocean, acetone mixing ratios are highest downwind of central America and central Africa. A comparison of the GISS ModelE2.1 results against twenty-six prior field measurements shows an overall great agreement, with a root mean squared error of 0.3494 and an R^2 value of 0.8306. To put these results into the context of model evaluation, a similar comparison to field measurements was done for the model's previous acetone scheme. The prior parameterization was designed as a rough representation of acetone oxidized from isoprene in the upper troposphere, without regard for realism near the surface, and this is evident from the comparison with surface observations: a root mean squared error and R^2 value of 1.3620 and 0.0413, respectively. The improvement of the new acetone tracer model in the GISS ModelE2.1 is evident from these statistics.

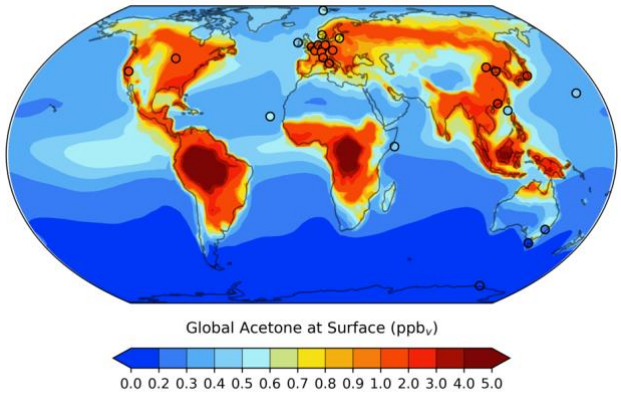

Figure 3. GISS ModelE2.1 spatial distribution of annual mean acetone at surface for the Baseline simulation. Filled circles represent data from twenty-six field measurements (de Gouw et al., 2004; Dolgorouky et al., 2012; Galbally et al., 2007; Guérette et al., 2019; Hu et al., 2013; Huang et al., 2020; Langford et al., 2010; Lewis et al., 2005; Li et al., 2019; Read et al., 2012; Schade & Goldstein, 2006; Singh et al., 2003; Solberg et al., 1996; Warneke & de Gouw, 2001; Yoshino et al., 2012; Yuan et al., 2013). The root mean squared error and the R^2 value between the Baseline acetone estimations and the field measurements are 0.3494 and 0.8306, respectively. A nonlinear colorbar is used to better differentiate the details in the map.

A breakdown of the acetone bidirectional fluxes indicates that its chemical production is concentrated over the continents, while chemical destruction is primarily over the oceans (Figure 4). Hotspots of production over the continents include the Southern and Eastern United States and central South America, East and Northern Asia, and Central Africa. Chemical sinks over the oceans are stronger in the tropics than in the high southern or northern latitudes. Annually, there is a net negative flux of about -20.46 Tg yr^{-1} (Figure 4). Observing the chemical flux over all four seasons, the net loss appears unaffected while the net source changes more significantly, following the seasonality of precursor compounds like isoprene and terpenes (Figure 5). Chemical production is strongest in the months of June/July/August, primarily in the US and Northern Asia. Production is weakest in the months of December/January/February, losing almost all production in the US and Northern Asia entirely. Still, a net negative flux is present for all four seasons (Figure 5).

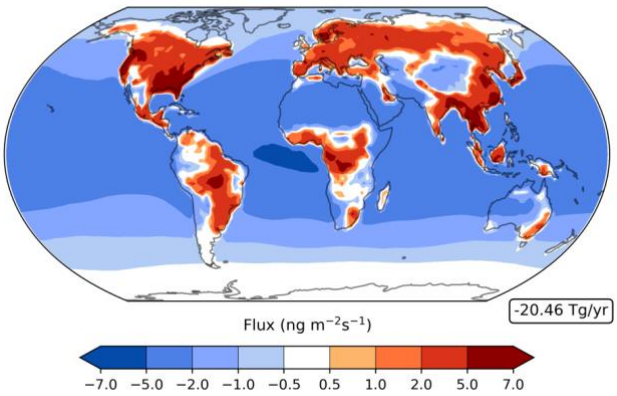

Figure 4. Annual average of acetone net chemistry fluxes (column-integrated) in the Baseline simulation, with red indicating a net source and blue indicating a net sink. A nonlinear colorbar is used to better differentiate the details in the map. The weighted global mean of the net chemistry flux is shown in a box on the lower right.

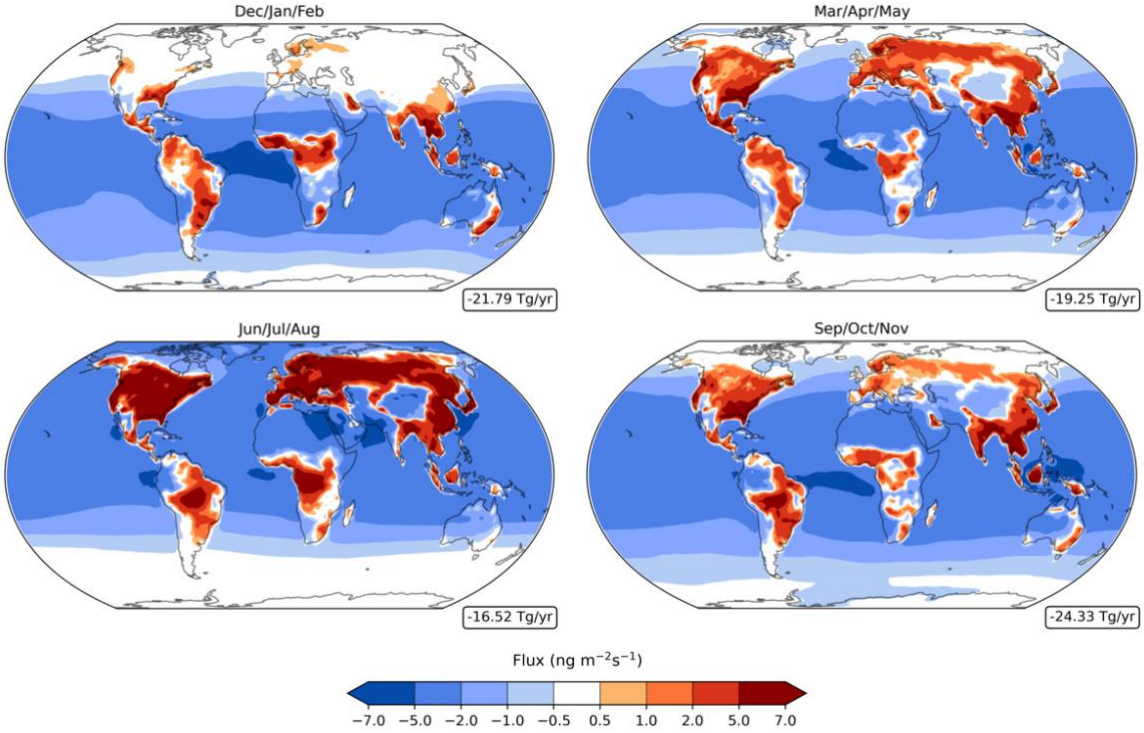

Figure 5. Acetone net chemistry fluxes (column-integrated) in the Baseline simulation for December-February (top left), March-May (top right), June-August (bottom left), and September-November (bottom right), with red indicating a net source and blue indicating a net sink. Nonlinear colorbars are used to better differentiate the details in the map. The weighted global means of the net chemistry fluxes are shown in boxes on the lower right.

The ocean acetone sources and sinks are unevenly distributed across latitudes. Oceanic uptake of acetone is mostly concentrated in the northern rather than the southern oceans, while the ocean acetone source is strongest in the tropics and decreases at higher latitudes of both hemispheres (Figure 6). Combining these two unidirectional fluxes results in the ocean serving as a sink in the northern high latitudes, a source in the tropical latitudes, and near neutral at the high southern latitudes (Figure 7). This finding

corroborates very well with findings from Fischer et al. (2012) and Wang et al. (2020). Oceanic bidirectional acetone fluxes present trends over the four seasons (Figure S2). Overall, every season has a positive global mean net flux. However, production becomes strongest in the months of December through May, and weakest in the months of June through November. Off the coast of western South America, the ocean appears to be a net sink of acetone, even though this latitude band is generally a source of acetone. This is especially evident in the months of June/July/August and September/October/November. As the model simulates this location to have high levels of acetone at the surface (Figure 3), we believe the acetone in the air is driving the ocean to be a sink there.

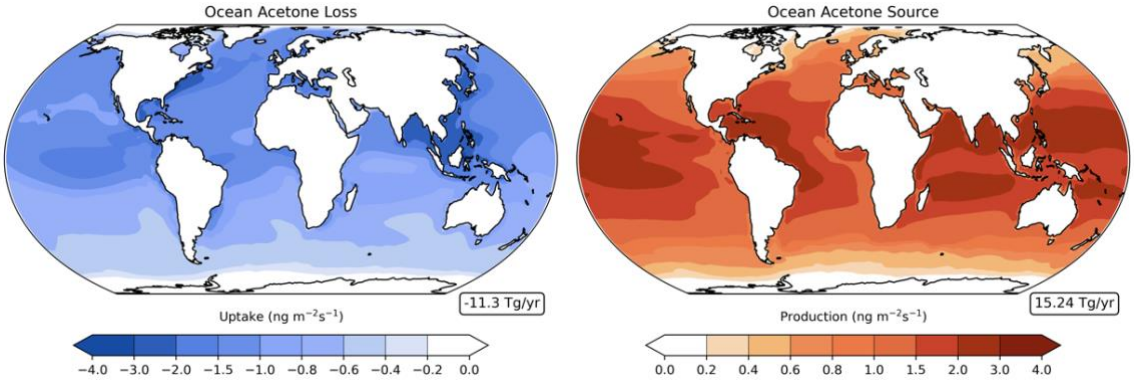

Figure 6. Annual average of the acetone ocean loss (left) and ocean source (right) in the Baseline simulation. Nonlinear colorbars are used to better differentiate the details in the map. The corresponding weighted global means of the ocean fluxes are shown in boxes on the lower right.

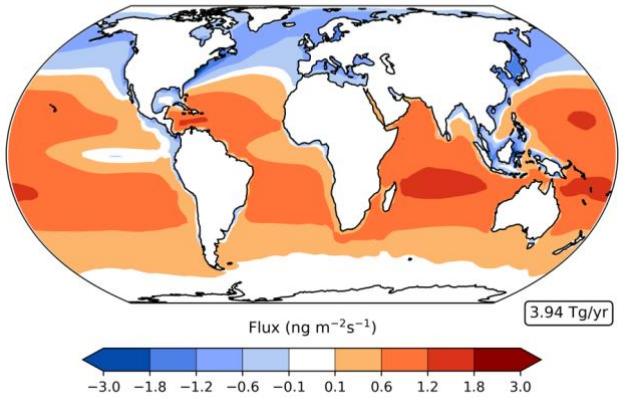

Figure 7. Annual average of acetone ocean bidirectional fluxes in the Baseline simulation, with red indicating a net source and blue indicating a net sink. A nonlinear colorbar is used to better differentiate the details in the map. The weighted global mean of the net chemistry flux is shown in a box on the lower right.

3.3 Vertical distribution of acetone

The vertical distribution of acetone varies by latitude, with near-surface air mixing ratios being higher in the tropics and in the northern midlatitudes. Acetone levels in the atmosphere decrease with height, a direct result of sinks dominating the sources (Figure 8). Prior to the implementation of an acetone tracer in the GISS ModelE2.1, when acetone was derived from the zonal mean of isoprene, the vertical distribution looked very different. Acetone was only concentrated around the tropics and did not extend nearly as high into the atmosphere. The complexity of Figure 8 supports the new acetone tracer scheme as a significant improvement to the GISS ModelE.

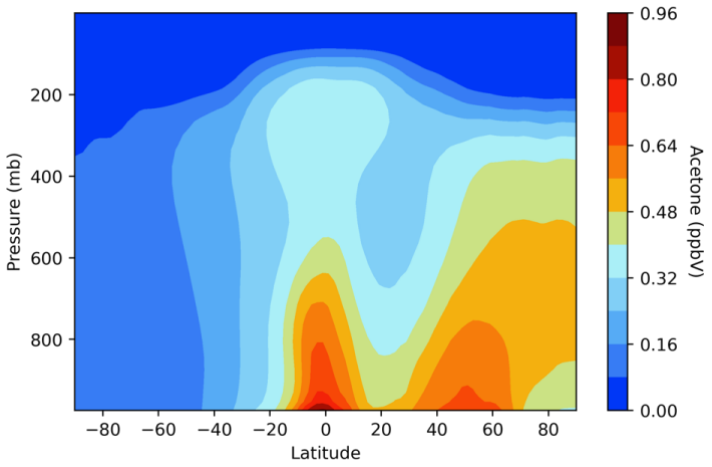

Figure 8. GISS ModelE2.1 vertical distribution of acetone air mixing ratios across latitudes in the Baseline simulation.

Another modelled vertical distribution of acetone, including a differentiation between two long seasons, is explored in Figure 9. In general, it was found that acetone mixing ratios are higher in the months of May-October than in November-April, and that this relationship is stronger in the lower atmosphere (0-2 km) than the upper atmosphere (6-10 km). This finding corroborated well with a similar analysis done by Fischer et al. (2012).

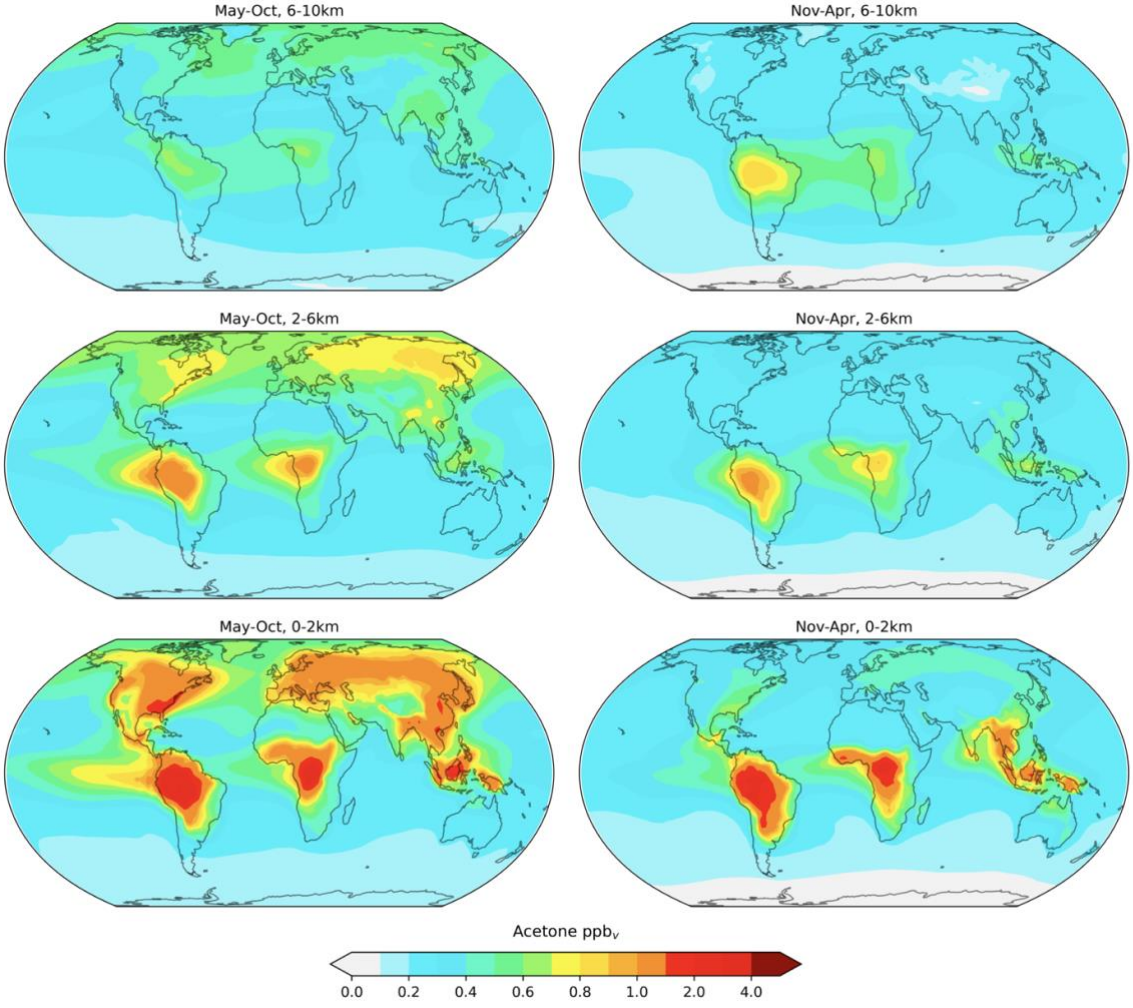

Figure 9. Baseline simulation acetone mixing ratios in the atmosphere at 0-2 km (bottom), 2-6 km (middle), and 6-10 km (top) for the months of May-October (left) and November-April (right). The mixing ratios in the vertical were averaged with an arithmetic mean. The choice of the slices and colors match those in Figure 1 by (Fischer et al., 2012).

Additionally, the GISS ModelE2.1 was compared to four ATom campaigns (Thompson et al., 2022) of acetone field measurements in the atmosphere (Apel et al., 2021). For this comparison, we averaged the flight data to the model grid, and then compared the resulting mean against the monthly mean fields of the model output. Contrary to other chemical species measured during ATom that vary significantly in space and time, acetone has a rather long lifetime, and the data are collected for the most part very far from its sources. Combining that with the fact that prescribed emissions in the model vary by month, not by day or even hour in GISS ModelE2.1, makes such a comparison appropriate. Meteorology though can affect long-range transport significantly, so for that reason we performed a nudged simulation (called Nudged_ATom) towards the MERRA-2 reanalysis (Gelaro et al., 2017), to capture such an effect more accurately. We also used emissions and greenhouse gas concentrations from the years of the ATom campaigns and varying with year, rather than the climatological means used in the Baseline simulation. Both the Nudged_ATom and Baseline simulations are plotted in the ATom comparisons presented here (Figure 10).

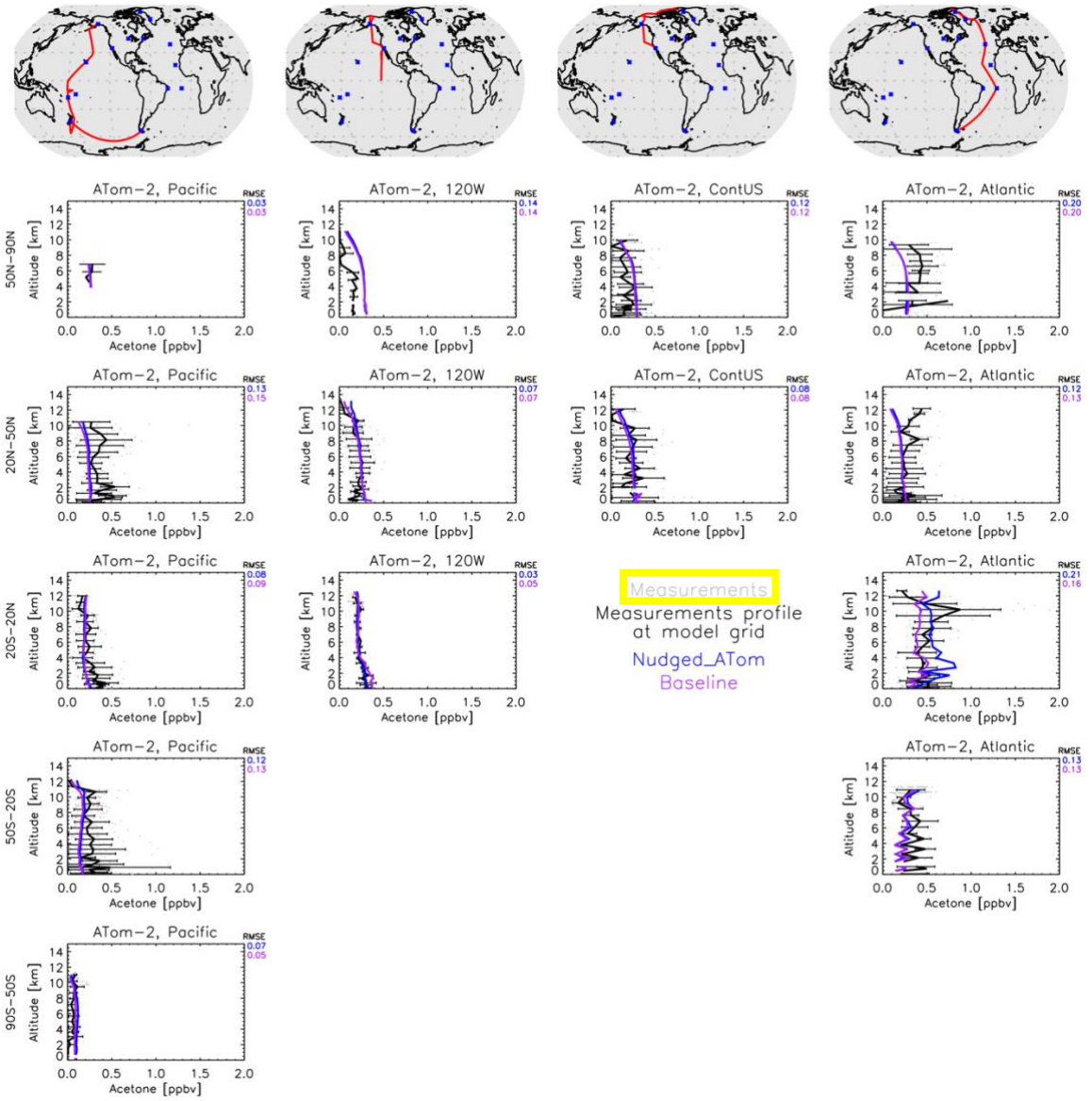

Figure 10. Comparison between the GISS ModelE2.1 simulations (Baseline in purple and Nudged_ATom in blue) and the ATom-2 field measurements (January-February 2017). Individual data points are shown with grey dots, and their average values are shown in black, with error bars representing the one-sigma range of the averages. The root mean square error (RMSE) of each simulation is shown at the top right of each plot.

There are very few notable differences between the nudged and climatological simulations. An example is the tropical Atlantic Ocean, where during ATom-2 (Figure 10), the nudged simulation calculates higher acetone concentrations, but without gain of skill. Both model simulations miss the upper tropospheric peak that is found in the measurements, likely indicating a missing long-range transported plume. Something similar is calculated during ATom-3 (Figure S4) for the southern Atlantic Ocean mid-latitudes, where the nudged simulation is higher. Contrary to the ATom-2 case, both simulations calculate an upper tropospheric maximum, which is not found in the measurements. The tropical and southern mid-latitude Atlantic Ocean regions are both downwind African biomass burning regions during ATom-2 and ATom-3, respectively, hinting to a primary and/or secondary incorrect source of acetone related with biomass burning and subsequent long-range transport. Other than those few cases, for the most part the two simulations are indistinguishable, indicating that our conclusions comparing climatological simulations to ATom should be robust. (Figures 10, and S3-S5). This is important to remember in Section 3.5.3, where we perform sensitivity analyses using climatological simulations and comparing against all four ATom campaigns.

3.4 Seasonality of acetone

Most European sites presented in Figure 3 have monthly-resolved measurements that can be used to analyze the seasonal behavior of acetone in the model (Figure 11, Figure S6) (Solberg et al., 1996). These sites differ with respect to their geographic locations and their proximity to anthropogenic sources. Zeppelin, Birkenes, Rucava, and Mace Head are all coastal sites, while Waldhof, Kosetice, Donon, Ispra, and Montelibretti are inland sites. Regarding anthropogenic sources, Zeppelin is the most remote location and Birkenes and Rucava each have small sources. Mace Head is a site affected by the marine boundary layer, and Waldhof, Kosetice and Donon are sites with small local anthropogenic sources that are generally located in higher emission regions. Montelibretti and particularly Ispra are subject to the highest anthropogenic sources. The measurements taken at Ispra show an opposite seasonality than what is expected, and previous studies have considered this anomalous (Jacob et al., 2002).

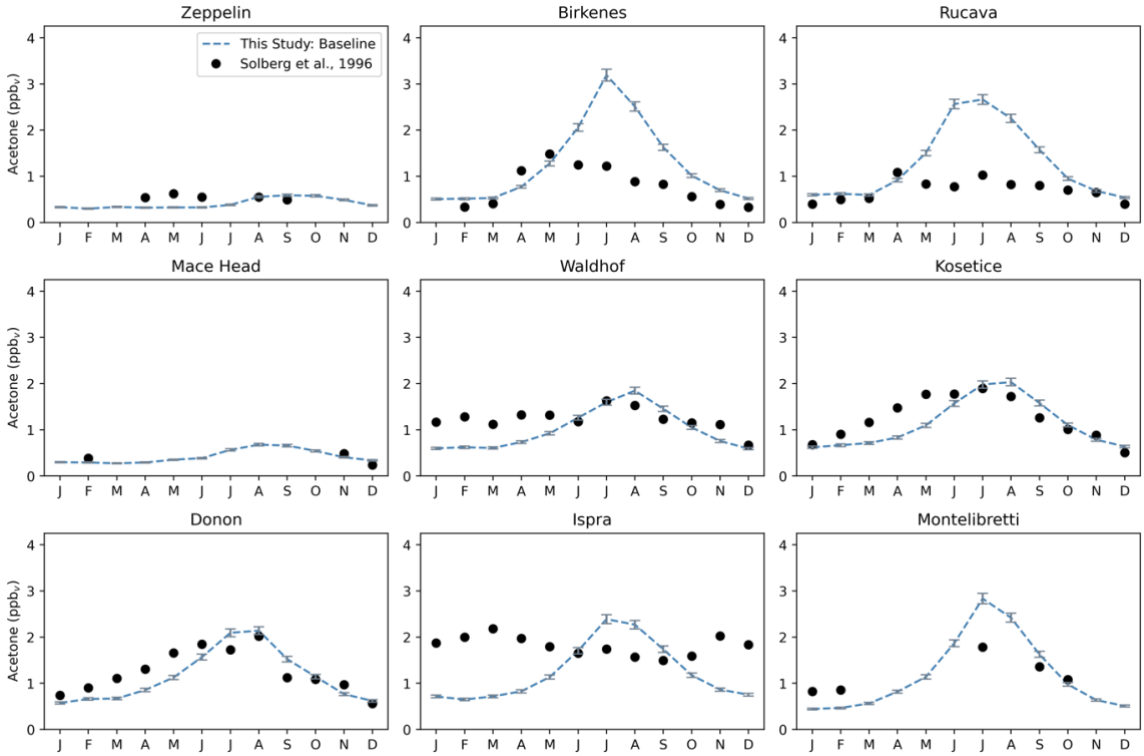

Figure 11. Acetone over twelve months at nine European sites, similar to that of Jacob et al. (2002). The modelled estimates of acetone at the surface from the Baseline simulation are shown as dashed blue lines and the grey error bars represent the one-sigma range of the modelled concentrations in the climatological mean of 5 years. Field measurements from Solberg et al., (1996) are shown as solid black dots. Root mean squared error between the Baseline simulation and field measurements are (left to right, top to bottom): 0.1968, 0.8714, 0.8724, 0.0914, 0.3907, 0.3430, 0.3160, 0.9454, 0.5454.

The GISS ModelE2.1 matches the seasonality of the measurements especially well in Zeppelin, Mace Head, Waldhof, Kosetice, and Donon; the average root mean square error between the Baseline model and the measurements at these five sites are 0.27. The Baseline model overestimates the measurements in Birkenes and Rucava (RMSE ≅ 0.87 for both), even though these two sites have low anthropogenic sources. This overestimation has been attributed to the vegetation source, which has a distinct seasonality and is much stronger than any other source there. Interestingly, in Montelibretti, the model's overestimation of vegetation, yet underestimation of local emissions, results in a decent estimation of the sources there (RMSE = 0.5454) (Figure 11).

As mentioned previously, an analysis of the distribution of the regional sources and sinks at the nine European sites shows that, except for Zeppelin and Mace Head, all studied European sites have vegetation as the dominant source that strongly contributes to the simulated seasonality of concentrations (Figure 12). Vegetation sources peak in the summer months and are lower in the winter. Deposition is a major sink of acetone that is comparable in magnitude with the vegetation source. Ocean uptake of acetone follows a weak seasonal cycle, being stronger in the summer months. The other fluxes (anthropogenic emissions, biomass burning and ocean production) do not exhibit much seasonality at these locations (Figure 12).

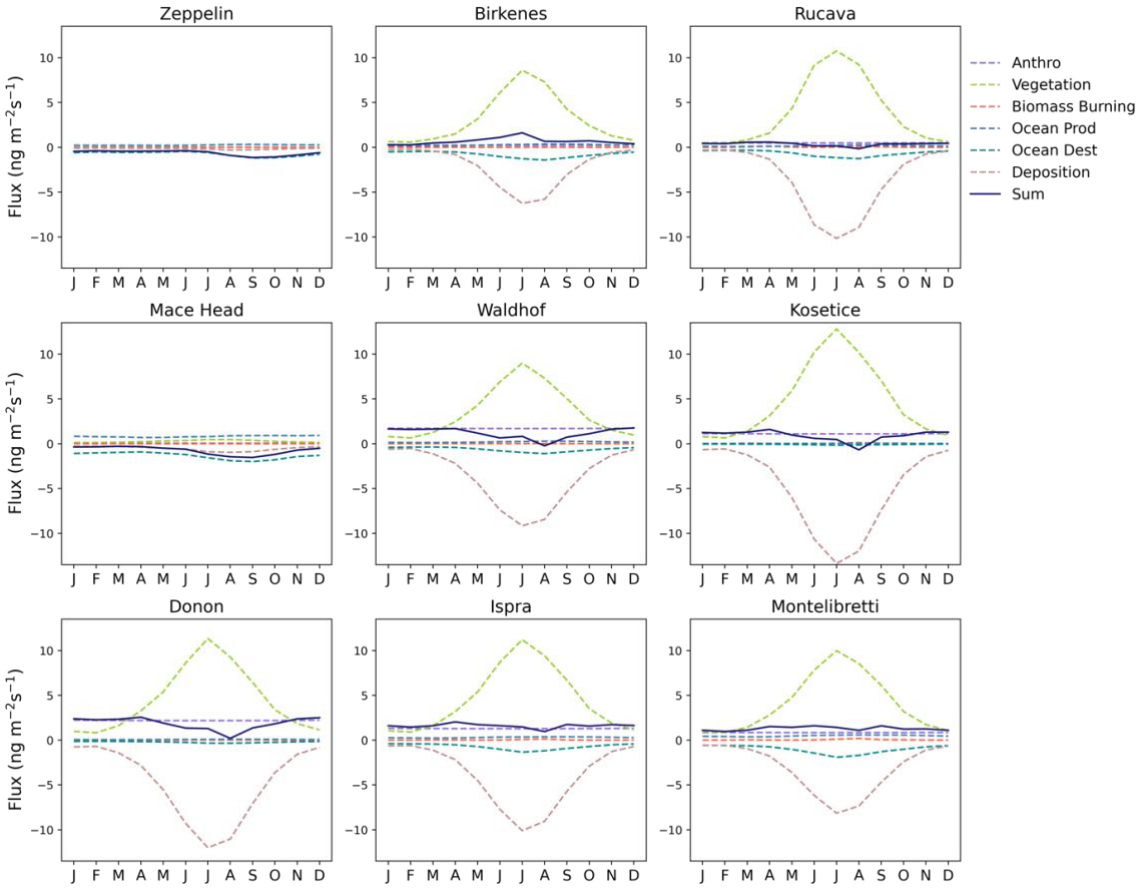

Figure 12. Contribution of acetone sources and sinks in the Baseline simulation over twelve months on the regional level (10˚ x 12.5˚ grid boxes) at nine European sites. The sources and sinks are shown as various colored dashed lines, and their sums are shown as a solid navy-blue lines.

We also compared the GISS ModelE2.1's surface acetone at observation sites with less temporal coverage (Figure 13). In general, the GISS ModelE2.1 matches the field measurements well. This is especially true for the non-summer seasons in Rosemount and Berkeley, and the summer peaks in Utrecht and Mainz. The model seems to be overestimating acetone around Australia, as shown by comparisons with Cape Grim and Wollongong, while underestimating emissions in large cities like Shenzhen, Beijing, London, and Paris.

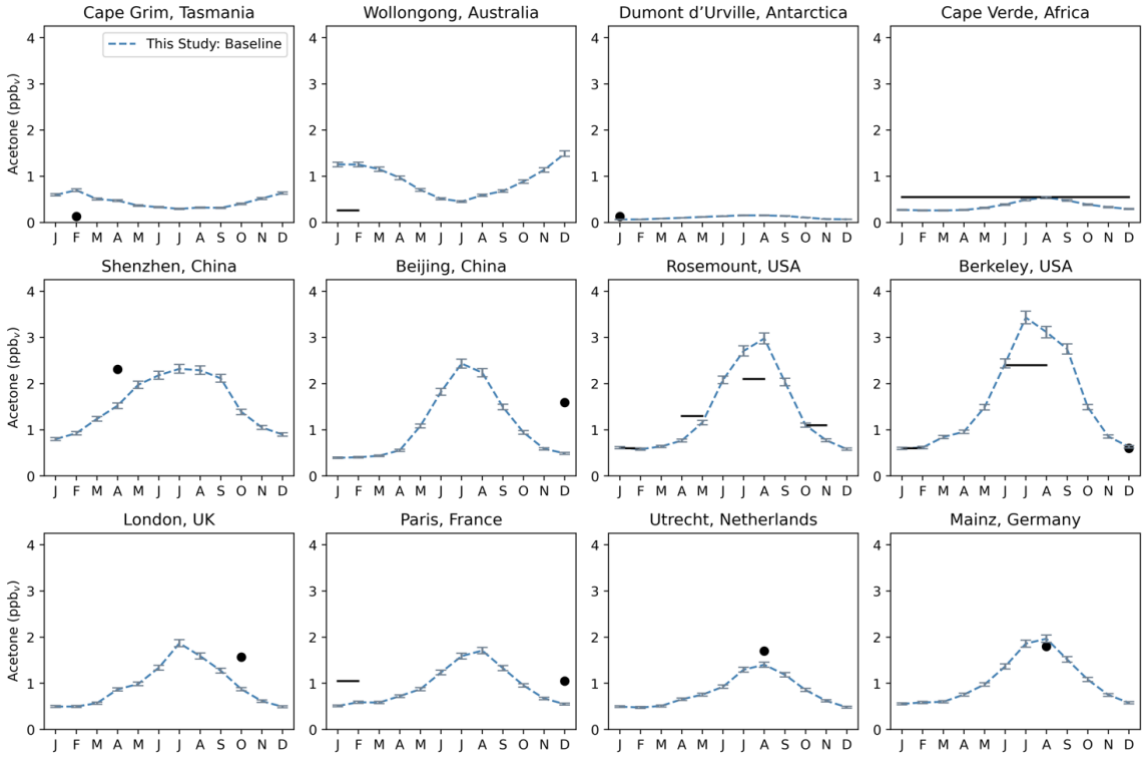

Figure 13. Acetone over twelve months for various sites that do not have enough measurements to resolve seasonality (Australia, Antarctica, Africa, Asia, Europe, North America). The modelled estimates of acetone at the surface from the Baseline simulation are shown as dashed blue lines and the grey error bars represent the one-sigma range of the modelled concentrations in the climatological mean of 5 years. The modelled estimates are overlaid with monthly (solid circles) or seasonal (solid lines) field measurements, as found in the literature (de Gouw et al., 2004; Dolgorouky et al., 2012; Galbally et al., 2007; Guérette et al., 2019; Hu et al., 2013; Huang et al., 2020; Langford et al., 2010; Legrand et al., 2012; Li et al., 2019; Read et al., 2012; Schade and Goldstein, 2006).

3.5 Sensitivity studies

The sensitivity simulations presented here have been described in section 2.5 and in Table 1. We grouped them in two categories: those directly related with chemical sources and sinks, and those related with terrestrial and oceanic acetone fluxes. Overall, the sensitivity studies that presented large changes to total atmospheric burden included Chem_Terp0, Chem_Par0.5, Chem_Par2.0, Veg_0.7, Ocn_2.0, and Dep_$f_0$0 (all but Chem_Cl0 and BB_2.0) (Figures S7-S12).

3.5.1 Chemistry

Chemistry sensitivity tests that modified the sources of acetone were analyzed with respect to the budget and global distribution of acetone. In the Chem_Cl0 simulation, where no acetone oxidation by the chlorine radical occurs, the overall global acetone budget does not change. However, in some places like Rucava, Ispra, Montelibretti, and Shenzhen, the shape of the acetone concentration profile over the year changes slightly (Figure 14, Figure S13). The Chem_Terp0 simulation that removes the production of acetone from terpenes decreases the summer peak of acetone by as much as 35.5% in Birkenes, 25.5% in Mainz, and 25.3% in Berkeley (Figure 14, Figure S13). Other sites like Montelibretti, Ispra and Paris have their summer peak decreased by 22.6%, 22.2%, and 19.0%, respectively (Figure 14, Figure S13). Coastal and remote areas like Zeppelin, Mace Head and Dumont d'Urville are not impacted by the removal of terpenes (Figure 14, Figure S13). There seems to be some nonlinearities

with the relationship between acetone abundance and its yield from paraffin, as the results from the Chem_Par2.0 and Chem_Par0.5 simulation reveal that doubling the yield has a stronger impact than halving it. For instance, in Montelibretti, doubling the yield from paraffin increases the summer peak by 35.7%, while halving the yield decreases the summer peak by only 8.3% (Figure 14, Figure S13). A similar relationship is observed at other sites: Ispra (19.1% increase with double paraffin, 2.5% decrease with half paraffin) and Berkeley (12.7% increase with double paraffin, 2.5% decrease with half paraffin) (Figure 14, Figure S13). Overall, we explored chemistry sensitivities that would tend to push acetone in both directions. The Baseline simulation falls between our tests, which we have identified as important uncertainties.

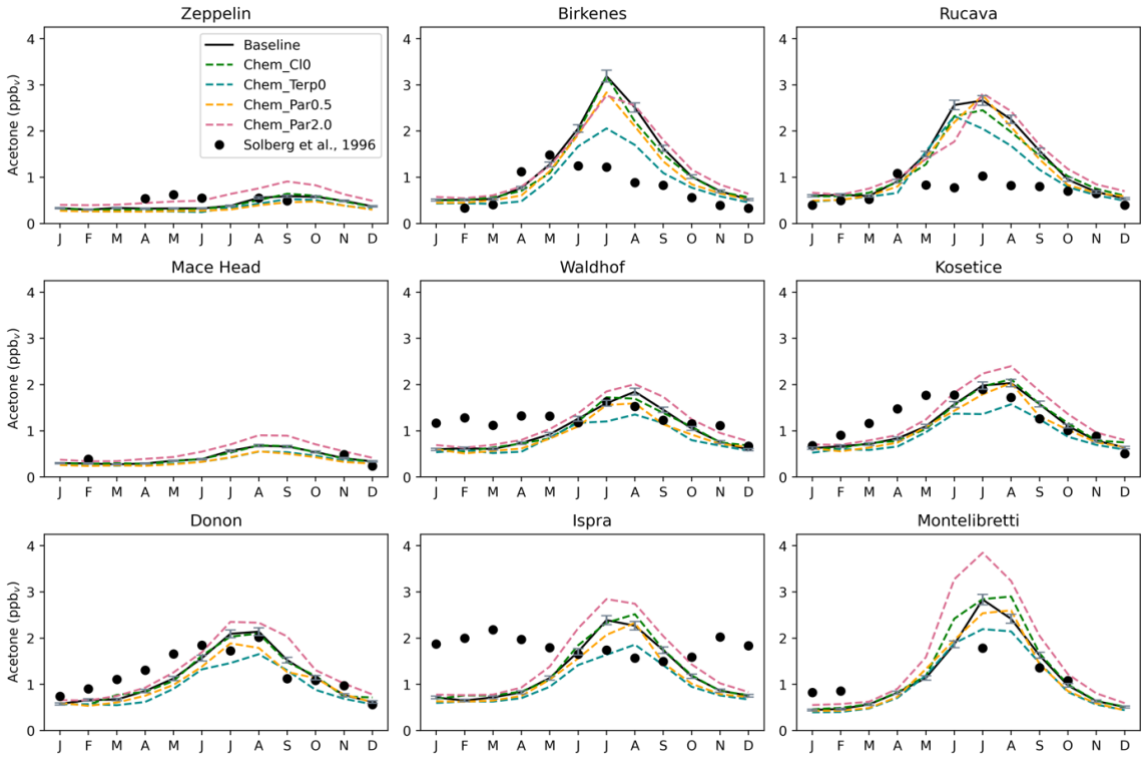

Figure 14. Similar to Figure 11, but with the chemistry sensitivity studies added. The modelled estimates of acetone at the surface from the Baseline simulation are shown as solid black lines, and the sensitivity studies are as follows: removing the acetone + chlorine reaction (dashed green lines), removing the production of acetone from terpenes (dashed blue lines), halving the yield of acetone from paraffin (dashed orange lines), and doubling the yield of acetone from paraffin (dashed pink lines). Field measurements from Solberg et al., (1996) are shown as solid black dots.

The spatial distribution differences between the chemistry sensitivity studies and the Baseline simulation show some interesting patterns (Figure 15). Removing the production of acetone from terpenes oxidation decreased acetone over the continents, and especially over tropical and boreal forests which are where terpenes are emitted. This change induced a feedback where acetone concentration increased slightly over the oceans (Figure 15, top left). Halving production of acetone from paraffin oxidation only decreased acetone concentrations over the continents (Figure 15, top right), while doubling it increased acetone concentrations over the continents but reduced it marginally downwind (Figure 15, bottom). Feedback resulting from this change was that acetone destruction increased over the tropics.

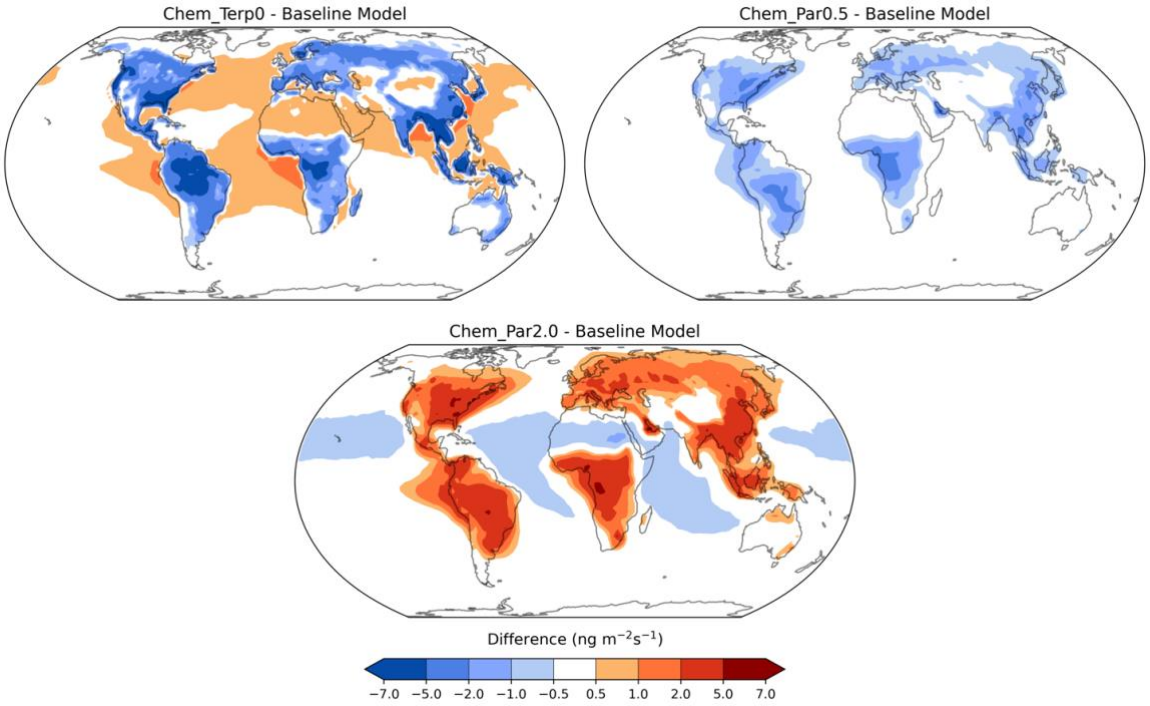

Figure 15. Chemistry sensitivities anomalies from Baseline, with red indicating an increase and blue indicating a decrease of the column-integrated net acetone chemistry flux. Nonlinear colorbars are used to better differentiate the details in the map. The fourth chemistry sensitivity study, Chem_Cl0, is omitted, since the changes everywhere are very small, less than 0.4 ng m^{-2} s^{-1}.

3.5.2 Terrestrial and oceanic fluxes

Terrestrial and oceanic fluxes sensitivities were analyzed at the same sites. The vegetation flux sensitivity, Veg_0.7, reduced acetone production from MEGAN by 30%. This change decreased the summer peak of acetone down at nearly every location studied, but most notably by 32.6% in Birkenes, 22.9% in Rucava, and 22.2% in Rosemount (Figure 16, Figure S14).

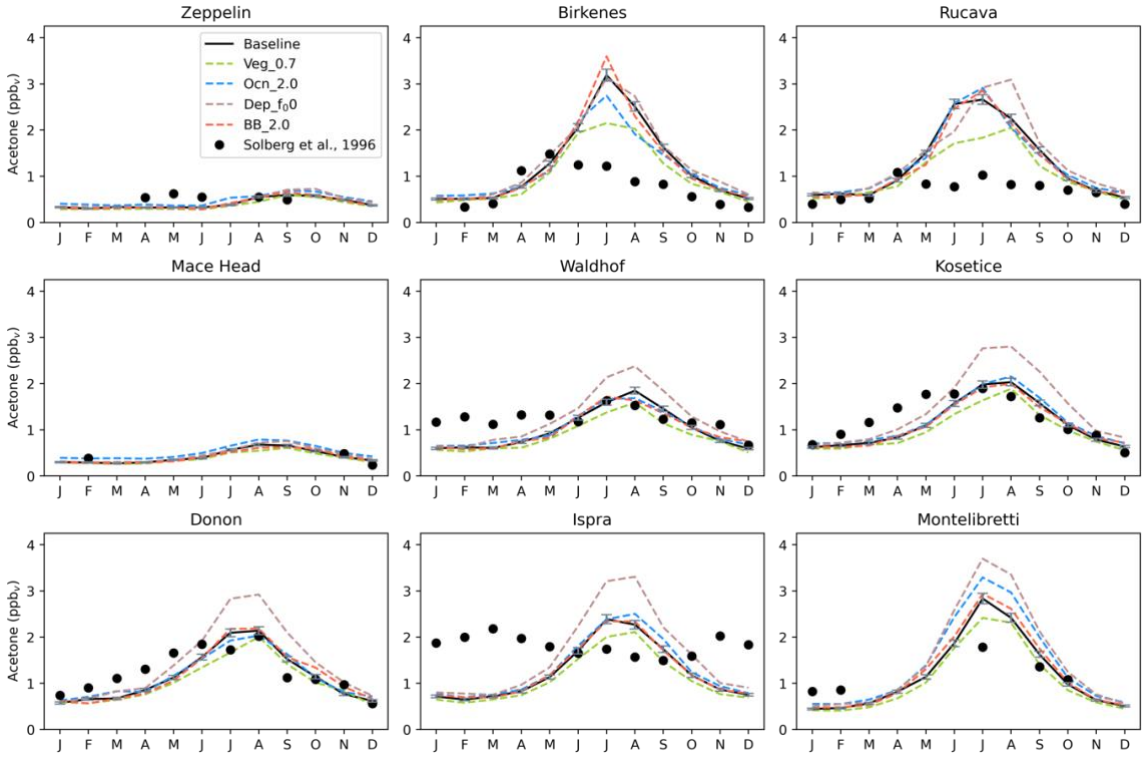

Figure 16. Similar to Figure 11, but with the terrestrial and oceanic sensitivity studies added. The modelled estimates of acetone at the surface from the Baseline simulation are shown as solid black lines, and the sensitivity studies are as follows: reducing vegetation emissions to 0.7 acetone from MEGAN (dashed light-green line), doubling ocean acetone concentration (dashed blue line), changing the reactivity factor for dry deposition (dashed brown line), and doubling biomass burning emissions (dashed orange line). Field measurements from Solberg et al., (1996) are shown as solid black dots.

In the oceanic flux sensitivity simulation, Ocn_2.0, the concentration of acetone in the water was doubled from 15 nM to 30 nM. The results of this simulation varied with geographic location. For instance, in Birkenes, doubling ocean concentration reduced overall acetone by 13.9%, while in Montelibretti, it was increased by 16.1% (Figure 16). Even though Birkenes is more of a coastal city than Montelibretti, this result may simply be a temperature effect; Birkenes is at 58°N, while Montelibretti is at 42°N, and a warmer ocean may produce more acetone. Overall, in most places, the doubling ocean acetone concentration did not change much atmospheric acetone throughout the year.

Another broader finding from the ocean sensitivity study is that doubling the ocean acetone concentration impacted oceanic emissions of acetone more than the oceanic uptake of acetone. Specifically, in this sensitivity study the emissions doubled while the uptake only increased by 40%. This difference may be attributed to the fact that a higher ocean concentration will generally cause less resistance in the emission direction, but more resistance in the uptake direction. The differences in oceanic acetone emissions and uptakes in this sensitivity study also resulted in increased chemical destruction, and an overall higher burden of acetone in the atmosphere (Figure S11).

In the dry deposition sensitivity simulation, the reactivity factor, f_0, was reduced from 0.1 to 0. As a result, the amount of acetone removed by deposition decreased, and the atmospheric acetone concentration increased. The strongest increases were found to be in Ispra (38.4% increase), Kosetice (37.9% increase), Paris (37.9% increase), Beijing (37.3% increase), Donon (36.6% increase),

Mainz (33.4% increase), Montelibretti (30.5% increase), Rosemount (28.9% increase), Berkeley (28.7% increase), and Waldhof (28.7% increase) (Figure 16, Figure S14). The final terrestrial fluxes sensitivity study, BB_2.0, doubled biomass burning emissions. This sensitivity did not significantly change acetone mixing ratios in any of the locations studied, except an increased summer spike (12.7% increase) in Birkenes (Figure 16). Most of the locations studied were far from biomass burning sites to begin with, however, so an analysis of this sensitivity study over biomass burning hotspots is needed.

The acetone concentration anomalies around the world between the terrestrial and oceanic fluxes sensitivity studies and the Baseline simulation are presented in Figure 17. Decreasing acetone production from MEGAN vegetation by 30% resulted in a decrease of acetone mixing ratios over the tropical and boreal forests, where this source is most prominent (Figure 17, top left). Doubling ocean acetone concentrations increased production of acetone from the oceans globally. This increase was stronger in the tropics, due to the higher sea surface temperatures (Figure 17, top right). Reducing the reactivity factor for dry deposition decreased the amount of acetone removed by deposition over the continents (Figure 17, bottom left), in particular where acetone concentration is elevated (Figure 3). Finally, doubling biomass burning emissions did not change acetone mixing ratios much, other than over biomass burning hotspots like central South America, central Africa, Southeast Asia, and Siberia (Figure 17, bottom right).

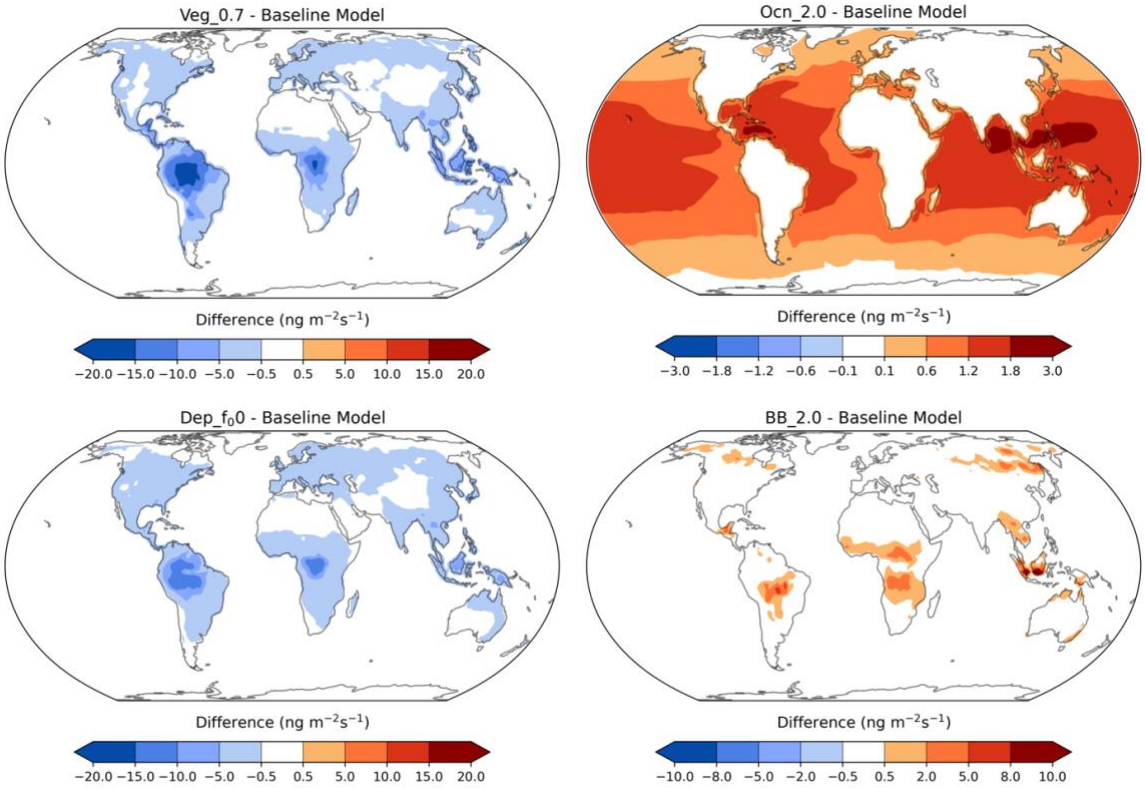

Figure 17. Acetone anomalies from the Baseline simulation for the vegetation (top left), ocean (top right), dry deposition (bottom left) and biomass burning (bottom right) sensitivities, with red indicating an increase and blue indicating a decrease of the specific flux. Nonlinear colorbars are used to better differentiate the details in the map.

3.5.3 ATom comparisons

The ATom comparisons were replicated with the sensitivity simulations (Figure 18, Figures S15-S17). Doubling the paraffin yield of acetone seemed to have the most noticeable impacts on the vertical profiles. As seen during ATom-1 (July-August

2016), doubling the paraffin yield decreases the root mean square error (RMSE) against measurements in the Northern hemisphere polar atmosphere (Figure 18) and brings the model to closer agreement to observations, but decreases the agreement throughout the remote Pacific Ocean, which implies different chemical formation pathways over the more polluted northern hemisphere on the Atlantic Ocean side, compared to the Pacific Ocean. Nearly the exact opposite is calculated in the case of the halving of the paraffin yield of acetone, which adds confidence to the chemical pathway explanation. The doubling of the ocean acetone concentration shows a small improvement (decrease) in the RMSE over the tropical and north Atlantic Ocean during ATom-1 and an even smaller decrease over the north hemisphere Pacific Ocean, but an increase over the tropical and south Pacific Ocean, showing the potential role of different ocean concentrations of acetone across the globe. It needs to be noted though that the model performs fairly well in those regions already, so the small improvements mentioned do not largely affect the regional acetone concentrations, as also expected due to the rather weak acetone source from the ocean.

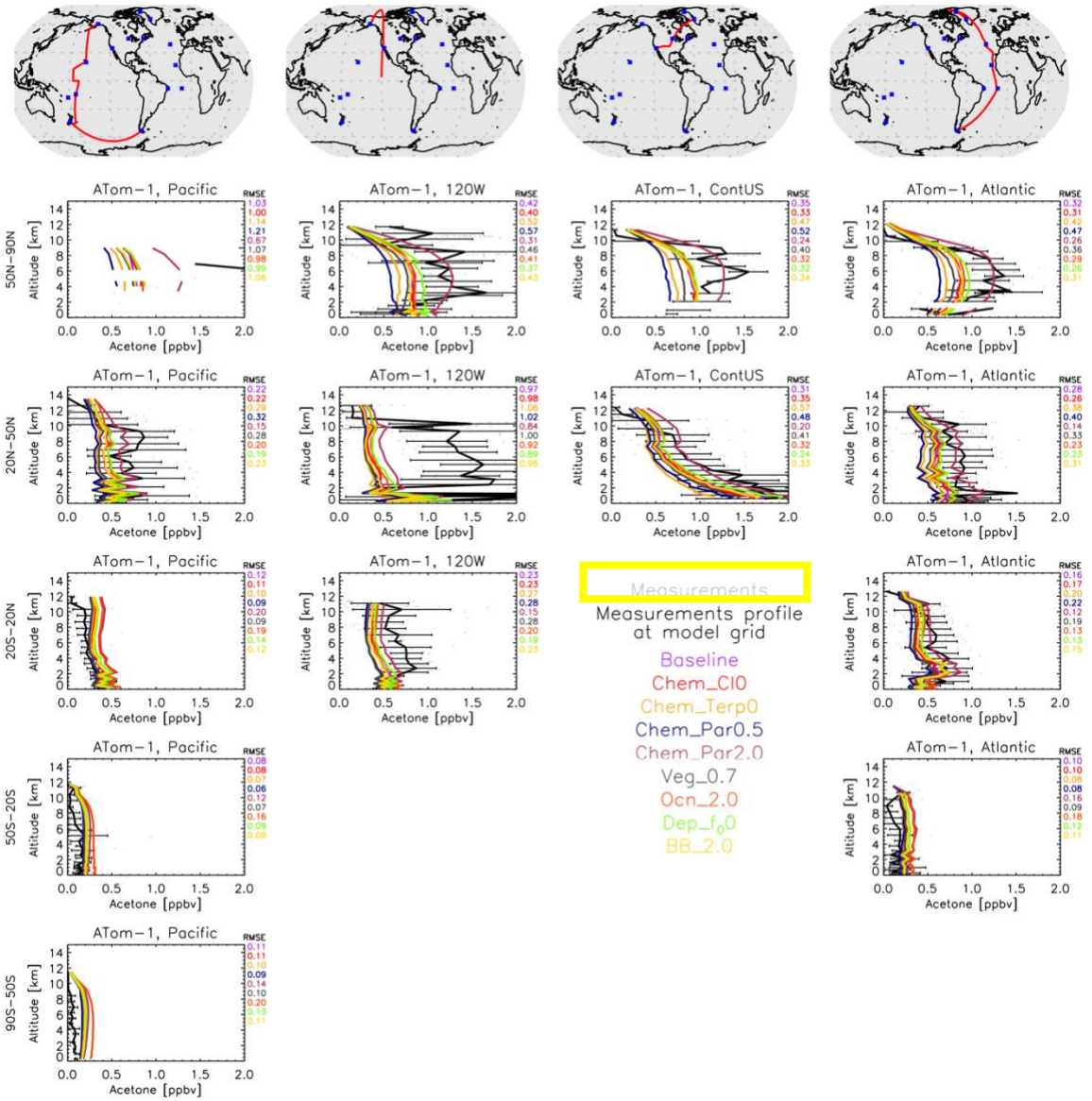

Figure 18. Similar to Figure 10, except a comparison between the GISS ModelE2.1 sensitivity simulations and the ATom-1 aircraft measurements (July-August 2016). Individual data points are shown with grey dots, and their average values are shown in black, with error bars representing the one-sigma range of the averages. The root mean square error (RMSE) of each simulation is shown

at the top right of each plot. Note that all sensitivities are to be compared against the Baseline simulation, not the Nudged_ATom one, but as shown earlier this makes very little difference in the comparison with observations (Figure 10).

The simulations of the boreal winter (January-February 2017) score the best against ATom-2. Acetone concentrations are the lowest during that period in both hemispheres, a direct result from the very low biomass burning emissions, which is among the highest acetone sources worldwide (Figure 2). In the region north of 50N, the increase of both the paraffin source and the oceanic source of acetone degrade the simulations, and the same applies for the measurements around 102W longitude, especially at mid-latitudes. The increase in oceanic source over the northern hemisphere mid-latitude Pacific Ocean improves (decreases) RMSE, but as already mentioned the low concentrations of acetone in that area (and in general during ATom-2) show that there is small sensitivity in the modified acetone sources to acetone profiles. While the ocean flux may be small, these ATom comparisons reveal that they especially matter in the southern latitudes. These are the same latitudes where the ocean appears to be in equilibrium (neither a strong source nor sink) (Figure 7).

During boreal fall (ATom-3), doubling the paraffin yield tends to overshoot most of the measurements (Figure S16), contrary to what was calculated during boreal summer (ATom-1; Figure 18). This is the case for most ATom-3 Atlantic Ocean flights, while an improvement is calculated when comparing with the flights near the west coast of the US or the Pacific Ocean mid-latitudes. These results reveal that the model may be underestimating a paraffin source during boreal summer, which diminishes during boreal fall.

The boreal spring season (April-May 2018; ATom-4; Figure S17) is the hardest for the model to simulate when it comes to northern hemisphere concentrations. All sensitivity studies greatly underestimate measurements, in particular the long-range transport upper tropospheric amount near the polar latitudes but also the concentrations measured throughout the troposphere at northern mid-latitudes. The model skillfully simulates tropical and southern hemisphere profiles, while it cannot reproduce the higher concentrations at northern latitudes. The increased yield from paraffin or the increased oceanic concentration do reduce RMSE, but still fall short on capturing the magnitude, or the shape, of the profiles of the spring hemisphere. We cannot infer from our model simulations whether this is a missing source or an underestimated sink, but the latter appears to be more plausible, given the large underestimation of all modeled profiles at northern mid-latitudes. In the southern hemisphere, the increase of oceanic acetone clearly degrades model skill, as was frequently the case during the other campaigns presented above. It is worth mentioning that for most cases the changes in the source of acetone do not alter the shape of the vertical profile. This means that the transport or chemical sinks of acetone dictate its spatiotemporal distribution more than sources, while the sources do affect the magnitude of that distribution, quite significantly under some of the conditions described here

4 Conclusion

The development of acetone's representation in the NASA GISS ModelE2.1 from its previous simplistic parameterization of instantaneous isoprene to a full tracer experiencing transport, chemistry, emissions, and deposition of its own, marks a significant improvement to the model's chemical scheme. Calculations of the 3-dimensional distribution of acetone as a function of time, as well as evaluations of its atmospheric burden and source/sink fluxes demonstrate the complexity of acetone's spatiotemporal distribution in the atmosphere. An extensive analysis was conducted to assess the simulated global acetone budget in the context of past modeling studies. Further comparisons were made against field measurements on a variety of spatial and temporal scales,

which indicated that the model agrees well with surface field measurements and vertical profiles in the remote atmosphere. The chemical formation of acetone from precursor compounds such as paraffin was found to be an uncertain yet impactful factor. Vegetation fluxes as calculated by MEGAN were identified as the dominant acetone source which dictates its seasonality. Additionally, the acetone concentration in seawater was found to affect oceanic sources more than oceanic sinks.

The work presented here demonstrates the usefulness of the approach to evaluate a chemical species in the model and can be used for similar evaluations of other important gaseous and aerosol species. Any feedback between acetone and the rest of the chemistry, and particularly ozone, have not been assessed here, and should be the goal of a future study. Additionally, the current ocean-acetone interaction uses a constant concentration of acetone in the ocean. It will be helpful to test a more realistic, non-uniform ocean acetone concentration, when this becomes available. Finally, other atmospheric conditions such as surface wind speed may be considered further when modifying the ocean scheme.

Code Availability

The GISS ModelE code is publicly available at https://simplex.giss.nasa.gov/snapshots/. The most recent public version is E.2.1.2; the version of the code used here is already committed in the non-public-facing repository and will be released in the future following the regular release cycle of ModelE, under version E3.1.

Data Availability

The 3-dimensional model output of acetone concentrations will be made public at the GISS website at the time of publication in the discussion phase, as was done in other publications (e.g. https://pubs.giss.nasa.gov/abs/ba08500g.html). This statement will be modified accordingly for final publication.

We have made available the simulated three-dimensional distributions of acetone from each simulation described in the paper (Baseline, sensitivity simulations in Table 1, and Nudged_ATom). These are found in zip files, grouped by simulation, here: https://doi.org/10.5281/zenodo.7567614. Each zip file contains a series of netCDF format files with filenames {month}_5yrAvg_Acetone_{simulation}.nc, where each file is a climatological average over 5 years of repeated forcing conditions.

The exception is the transient-forcing simulation "Nudged_ATom", which contains single-month averages of acetone from JUL 2016 through MAY 2018, to cover the ATom observational period. The file names for that simulation are of the form: {month}_{year}_Acetone_Nudged_ATom.nc. Acetone is in ppb_v units and given on the model's native grid and vertical levels. These are hybrid sigma levels, but nominal pressure middles and edges are given in the plm and ple variables, respectively, and the grid box surface areas are also provided.

Author Contribution

KT conceived the study and guided the model development which was done by GF. All simulations presented here were performed by GF. DS advised during the whole development process. AR did the literature search and all comparisons against other modeling studies. With the exception of the ATom analysis and plots which were done by KT, and comparisons against field measurements

and the rest of the plots were done by AR. AR drafted the first version of the manuscript, and all authors contributed to it. GF prepared all model outputs for dissemination.

Competing Interests

The authors declare that they have no conflict of interest.

Acknowledgements

Climate modeling at GISS is supported by the NASA Modeling, Analysis and Prediction program. AR acknowledges support from North Carolina Space Grant and the NASA Office of STEM Engagement. Resources supporting this work were provided by the NASA High-End Computing (HEC) Program through the NASA Center for Climate Simulation (NCCS) at Goddard Space Flight Center.

References

Apel, E. C., Asher, E. C., Hills, A. J., and Hornbrook, R. S.: ATom: Volatile Organic Compounds (VOCs) from the TOGA instrument, Version 2, ORNL DAAC, https://doi.org/10.3334/ORNLDAAC/1936, 2021.

Arnold, S. R., Chipperfield, M. P., and Blitz, M. A.: A three-dimensional model study of the effect of new temperature-dependent quantum yields for acetone photolysis, J. Geophys. Res. Atmospheres, 110, https://doi.org/10.1029/2005JD005998, 2005.

Beale, R., Dixon, J. L., Arnold, S. R., Liss, P. S., and Nightingale, P. D.: Methanol, acetaldehyde, and acetone in the surface waters of the Atlantic Ocean, J. Geophys. Res. Oceans, 118, 5412–5425, https://doi.org/10.1002/jgrc.20322, 2013.

Benkelberg, H.-J., Hamm, S., and Warneck, P.: Henry's law coefficients for aqueous solutions of acetone, acetaldehyde and acetonitrile, and equilibrium constants for the addition compounds of acetone and acetaldehyde with bisulfite, J. Atmospheric Chem., 20, 17–34, https://doi.org/10.1007/BF01099916, 1995.

Brewer, J. F., Bishop, M., Kelp, M., Keller, C. A., Ravishankara, A. R., and Fischer, E. V.: A sensitivity analysis of key natural factors in the modeled global acetone budget, J. Geophys. Res. Atmospheres, 122, 2043–2058, https://doi.org/10.1002/2016JD025935, 2017.

Chin, M., Jacob, D. J., Gardner, G. M., Foreman-Fowler, M. S., Spiro, P. A., and Savoie, D. L.: A global three-dimensional model of tropospheric sulfate, J. Geophys. Res. Atmospheres, 101, 18667–18690, https://doi.org/10.1029/96JD01221, 1996.

Dolgorouky, C., Gros, V., Sarda-Esteve, R., Sinha, V., Williams, J., Marchand, N., Sauvage, S., Poulain, L., Sciare, J., and Bonsang, B.: Total OH reactivity measurements in Paris during the 2010 MEGAPOLI winter campaign, Atmospheric Chem. Phys., 12, 9593–9612, https://doi.org/10.5194/acp-12-9593-2012, 2012.

Dufour, G., Szopa, S., Harrison, J. J., Boone, C. D., and Bernath, P. F.: Seasonal variations of acetone in the upper troposphere–lower stratosphere of the northern midlatitudes as observed by ACE-FTS, J. Mol. Spectrosc., 323, 67–77, https://doi.org/10.1016/j.jms.2016.02.006, 2016.

Elias, T., Szopa, S., Zahn, A., Schuck, T., Brenninkmeijer, C., Sprung, D., and Slemr, F.: Acetone variability in the upper troposphere: analysis of CARIBIC observations and LMDz-INCA chemistry-climate model simulations, Atmospheric Chem. Phys., 11, 8053–8074, https://doi.org/10.5194/acp-11-8053-2011, 2011.

Fischbeck, G., Bönisch, H., Neumaier, M., Brenninkmeijer, C. A. M., Orphal, J., Brito, J., Becker, J., Sprung, D., van Velthoven, P. F. J., and Zahn, A.: Acetone–CO enhancement ratios in the upper troposphere based on 7 years of CARIBIC data: new insights and estimates of regional acetone fluxes, Atmospheric Chem. Phys., 17, 1985–2008, https://doi.org/10.5194/acp-17-1985-2017, 2017.

Fischer, E. V., Jacob, D. J., Millet, D. B., Yantosca, R. M., and Mao, J.: The role of the ocean in the global atmospheric budget of acetone, Geophys. Res. Lett., 39, https://doi.org/10.1029/2011GL050086, 2012.

Folberth, G. A., Hauglustaine, D. A., Lathière, J., and Brocheton, F.: Interactive chemistry in the Laboratoire de Météorologie Dynamique general circulation model: model description and impact analysis of biogenic hydrocarbons on tropospheric chemistry, Atmospheric Chem. Phys., 6, 2273–2319, https://doi.org/10.5194/acp-6-2273-2006, 2006.

Fujimori, S., Hasegawa, T., Masui, T., Takahashi, K., Herran, D. S., Dai, H., Hijioka, Y., and Kainuma, M.: SSP3: AIM implementation of Shared Socioeconomic Pathways, Glob. Environ. Change, 42, 268–283, https://doi.org/10.1016/j.gloenvcha.2016.06.009, 2017.

Galbally, I., Lawson, S. J., Bentley, S., Gillett, R., Meyer, M., and Goldstein, A.: Volatile organic compounds in marine air at Cape Grim, Australia, Environ. Chem. - Env. CHEM, 4, https://doi.org/10.1071/EN07024, 2007.

Gelaro, R., McCarty, W., Suárez, M. J., Todling, R., Molod, A., Takacs, L., Randles, C. A., Darmenov, A., Bosilovich, M. G., Reichle, R., Wargan, K., Coy, L., Cullather, R., Draper, C., Akella, S., Buchard, V., Conaty, A., Silva, A. M. da, Gu, W., Kim, G.-K., Koster, R., Lucchesi, R., Merkova, D., Nielsen, J. E., Partyka, G., Pawson, S., Putman, W., Rienecker, M., Schubert, S. D., Sienkiewicz, M., and Zhao, B.: The Modern-Era Retrospective Analysis for Research and Applications, Version 2 (MERRA-2), J. Clim., 30, 5419–5454, https://doi.org/10.1175/JCLI-D-16-0758.1, 2017.

de Gouw, J., Warneke, C., Holzinger, R., Klüpfel, T., and Williams, J.: Inter-comparison between airborne measurements of methanol, acetonitrile and acetone using two differently configured PTR-MS instruments, Int. J. Mass Spectrom., 239, 129–137, https://doi.org/10.1016/j.ijms.2004.07.025, 2004.

Guenther, A. B., Jiang, X., Heald, C. L., Sakulyanontvittaya, T., Duhl, T., Emmons, L. K., and Wang, X.: The Model of Emissions of Gases and Aerosols from Nature version 2.1 (MEGAN2.1): an extended and updated framework for modeling biogenic emissions, Geosci. Model Dev., 5, 1471–1492, https://doi.org/10.5194/gmd-5-1471-2012, 2012.

Guérette, É.-A., Paton-Walsh, C., Galbally, I., Molloy, S., Lawson, S., Kubistin, D., Buchholz, R., Griffith, D. W. T., Langenfelds, R. L., Krummel, P. B., Loh, Z., Chambers, S., Griffiths, A., Keywood, M., Selleck, P., Dominick, D., Humphries, R., and Wilson, S. R.: Composition of Clean Marine Air and Biogenic Influences on VOCs during the MUMBA Campaign, Atmosphere, 10, 383, https://doi.org/10.3390/atmos10070383, 2019.

Hoesly, R. M., Smith, S. J., Feng, L., Klimont, Z., Janssens-Maenhout, G., Pitkanen, T., Seibert, J. J., Vu, L., Andres, R. J., Bolt, R. M., Bond, T. C., Dawidowski, L., Kholod, N., Kurokawa, J., Li, M., Liu, L., Lu, Z., Moura, M. C. P., O'Rourke, P. R., and Zhang, Q.: Historical (1750–2014) anthropogenic emissions of reactive gases and aerosols from the Community Emissions Data System (CEDS), Geosci. Model Dev., 11, 369–408, https://doi.org/10.5194/gmd-11-369-2018, 2018.

Hu, L., Millet, D. B., Kim, S. Y., Wells, K. C., Griffis, T. J., Fischer, E. V., Helmig, D., Hueber, J., and Curtis, A. J.: North American acetone sources determined from tall tower measurements and inverse modeling, Atmospheric Chem. Phys., 13, 3379–3392, https://doi.org/10.5194/acp-13-3379-2013, 2013.

Huang, X.-F., Zhang, B., Xia, S.-Y., Han, Y., Wang, C., Yu, G.-H., and Feng, N.: Sources of oxygenated volatile organic compounds (OVOCs) in urban atmospheres in North and South China, Environ. Pollut., 261, 114152, https://doi.org/10.1016/j.envpol.2020.114152, 2020.

Jacob, D. J., Field, B. D., Jin, E. M., Bey, I., Li, Q., Logan, J. A., Yantosca, R. M., and Singh, H. B.: Atmospheric budget of acetone, J. Geophys. Res. Atmospheres, 107, ACH 5-1-ACH 5-17, https://doi.org/10.1029/2001JD000694, 2002.

Johnson, M. T.: A numerical scheme to calculate temperature and salinity dependent air-water transfer velocities for any gas, Ocean Sci., 6, 913–932, https://doi.org/10.5194/os-6-913-2010, 2010.

Kelley, M., Schmidt, G. A., Nazarenko, L. S., Bauer, S. E., Ruedy, R., Russell, G. L., Ackerman, A. S., Aleinov, I., Bauer, M., Bleck, R., Canuto, V., Cesana, G., Cheng, Y., Clune, T. L., Cook, B. I., Cruz, C. A., Genio, A. D. D., Elsaesser, G. S., Faluvegi, G., Kiang, N. Y., Kim, D., Lacis, A. A., Leboissetier, A., LeGrande, A. N., Lo, K. K., Marshall, J., Matthews, E. E., McDermid, S., Mezuman, K., Miller, R. L., Murray, L. T., Oinas, V., Orbe, C., García-Pando, C. P., Perlwitz, J. P., Puma, M. J., Rind, D., Romanou, A., Shindell, D. T., Sun, S., Tausnev, N., Tsigaridis, K., Tselioudis, G., Weng, E., Wu, J., and Yao, M.-S.: GISS-E2.1: Configurations and Climatology, J. Adv. Model. Earth Syst., 12, e2019MS002025, https://doi.org/10.1029/2019MS002025, 2020.

Khan, M. A. H., Cooke, M. C., Utembe, S. R., Archibald, A. T., Maxwell, P., Morris, W. C., Xiao, P., Derwent, R. G., Jenkin, M. E., Percival, C. J., Walsh, R. C., Young, T. D. S., Simmonds, P. G., Nickless, G., O'Doherty, S., and Shallcross, D. E.: A study of global atmospheric budget and distribution of acetone using global atmospheric model STOCHEM-CRI, Atmos. Environ., 112, 269–277, https://doi.org/10.1016/j.atmosenv.2015.04.056, 2015.

Koch, D., Jacob, D., Tegen, I., Rind, D., and Chin, M.: Tropospheric sulfur simulation and sulfate direct radiative forcing in the Goddard Institute for Space Studies general circulation model, J. Geophys. Res. Atmospheres, 104, 23799–23822, https://doi.org/10.1029/1999JD900248, 1999.

Langford, B., Nemitz, E., House, E., Phillips, G. J., Famulari, D., Davison, B., Hopkins, J. R., Lewis, A. C., and Hewitt, C. N.: Fluxes and concentrations of volatile organic compounds above central London, UK, Atmospheric Chem. Phys., 10, 627–645, https://doi.org/10.5194/acp-10-627-2010, 2010.

Legrand, M., Gros, V., Preunkert, S., Sarda-Estève, R., Thierry, A.-M., Pépy, G., and Jourdain, B.: A reassessment of the budget of formic and acetic acids in the boundary layer at Dumont d'Urville (coastal Antarctica): The role of penguin emissions on the budget of several oxygenated volatile organic compounds, J. Geophys. Res. Atmospheres, 117, https://doi.org/10.1029/2011JD017102, 2012.

Lewis, A. C., Hopkins, J. R., Carpenter, L. J., Stanton, J., Read, K. A., and Pilling, M. J.: Sources and sinks of acetone, methanol, and acetaldehyde in North Atlantic marine air, Atmospheric Chem. Phys., 5, 1963–1974, https://doi.org/10.5194/acp-5-1963-2005, 2005.

Li, K., Li, J., Tong, S., Wang, W., Huang, R.-J., and Ge, M.: Characteristics of wintertime VOCs in suburban and urban Beijing: concentrations, emission ratios, and festival effects, Atmospheric Chem. Phys., 19, 8021–8036, https://doi.org/10.5194/acp-19-8021-2019, 2019.

Liss, P. S. and Slater, P. G.: Flux of Gases across the Air-Sea Interface, Nature, 247, 181–184, https://doi.org/10.1038/247181a0, 1974.

Marandino, C. A., Bruyn, W. J. D., Miller, S. D., Prather, M. J., and Saltzman, E. S.: Oceanic uptake and the global atmospheric acetone budget, Geophys. Res. Lett., 32, https://doi.org/10.1029/2005GL023285, 2005.

van Marle, M. J. E., Kloster, S., Magi, B. I., Marlon, J. R., Daniau, A.-L., Field, R. D., Arneth, A., Forrest, M., Hantson, S., Kehrwald, N. M., Knorr, W., Lasslop, G., Li, F., Mangeon, S., Yue, C., Kaiser, J. W., and van der Werf, G. R.: Historic global biomass burning emissions for CMIP6 (BB4CMIP) based on merging satellite observations with proxies and fire models (1750–2015), Geosci. Model Dev., 10, 3329–3357, https://doi.org/10.5194/gmd-10-3329-2017, 2017.

Neu, J. L., Prather, M. J., and Penner, J. E.: Global atmospheric chemistry: Integrating over fractional cloud cover, J. Geophys. Res. Atmospheres, 112, 2006JD008007, https://doi.org/10.1029/2006JD008007, 2007.

O'Rourke, P. R., Smith, S. J., Mott, A., Ahsan, H., McDuffie, E. E., Crippa, M., Klimont, Z., McDonald, B., Wang, S., Nicholson, M. B., Feng, L., and Hoesly, R. M.: CEDS v_2021_04_21 Release Emission Data, https://doi.org/10.5281/zenodo.4741285, 2021.

Read, K. A., Carpenter, L. J., Arnold, S. R., Beale, R., Nightingale, P. D., Hopkins, J. R., Lewis, A. C., Lee, J. D., Mendes, L., and Pickering, S. J.: Multiannual Observations of Acetone, Methanol, and Acetaldehyde in Remote Tropical Atlantic Air: Implications for Atmospheric OVOC Budgets and Oxidative Capacity, Environ. Sci. Technol., 46, 11028–11039, https://doi.org/10.1021/es302082p, 2012.

Riahi, K., van Vuuren, D. P., Kriegler, E., Edmonds, J., O'Neill, B. C., Fujimori, S., Bauer, N., Calvin, K., Dellink, R., Fricko, O., Lutz, W., Popp, A., Cuaresma, J. C., Kc, S., Leimbach, M., Jiang, L., Kram, T., Rao, S., Emmerling, J., Ebi, K., Hasegawa, T., Havlik, P., Humpenöder, F., Da Silva, L. A., Smith, S., Stehfest, E., Bosetti, V., Eom, J., Gernaat, D., Masui, T., Rogelj, J., Strefler, J., Drouet, L., Krey, V., Luderer, G., Harmsen, M., Takahashi, K., Baumstark, L., Doelman, J. C., Kainuma, M., Klimont, Z., Marangoni, G., Lotze-Campen, H., Obersteiner, M., Tabeau, A., and Tavoni, M.: The Shared Socioeconomic Pathways and their energy, land use, and greenhouse gas emissions implications: An overview, Glob. Environ. Change, 42, 153–168, https://doi.org/10.1016/j.gloenvcha.2016.05.009, 2017.

Sander, R.: Compilation of Henry's Law Constants for Inorganic and Organic Species of Potential Importance in Environmental Chemistry, 1999.

Sander, S. P., J Abbatt, J. R. Barker, J. B. Burkholder, R. R. Friedl, D. M. Golden, R. E. Huie, C. E. Kolb, M. J. Kurylo, G. K. Moortgat, V. L. Orkin, and P. H. Wine: Chemical Kinetics and Photochemical Data for Use in Atmospheric Studies Evaluation No. 17, JPL Publication 10-6, Jet Propulsion Laboratory, Pasadena, 2011.

Schade, G. W. and Goldstein, A. H.: Seasonal measurements of acetone and methanol: Abundances and implications for atmospheric budgets, Glob. Biogeochem. Cycles, 20, https://doi.org/10.1029/2005GB002566, 2006.

Shindell, D. T., Grenfell, J. L., Rind, D., Grewe, V., and Price, C.: Chemistry-climate interactions in the Goddard Institute for Space Studies general circulation model: 1. Tropospheric chemistry model description and evaluation, J. Geophys. Res. Atmospheres, 106, 8047–8075, https://doi.org/10.1029/2000JD900704, 2001.

Shindell, D. T., Faluvegi, G., and Bell, N.: Preindustrial-to-present-day radiative forcing by tropospheric ozone from improved simulations with the GISS chemistry-climate GCM, Atmospheric Chem. Phys., 3, 1675–1702, https://doi.org/10.5194/acp-3-1675-2003, 2003.

Singh, H., Chen, Y., Tabazadeh, A., Fukui, Y., Bey, I., Yantosca, R., Jacob, D., Arnold, F., Wohlfrom, K., Atlas, E., Flocke, F., Blake, D., Blake, N., Heikes, B., Snow, J., Talbot, R., Gregory, G., Sachse, G., Vay, S., and Kondo, Y.: Distribution and fate of selected oxygenated organic species in the troposphere and lower stratosphere over the Atlantic, J. Geophys. Res. Atmospheres, 105, 3795–3805, https://doi.org/10.1029/1999JD900779, 2000.

Singh, H. B., O'Hara, D., Herlth, D., Sachse, W., Blake, D. R., Bradshaw, J. D., Kanakidou, M., and Crutzen, P. J.: Acetone in the atmosphere: Distribution, sources, and sinks, J. Geophys. Res. Atmospheres, 99, 1805–1819, https://doi.org/10.1029/93JD00764, 1994.

Singh, H. B., Tabazadeh, A., Evans, M. J., Field, B. D., Jacob, D. J., Sachse, G., Crawford, J. H., Shetter, R., and Brune, W. H.: Oxygenated volatile organic chemicals in the oceans: Inferences and implications based on atmospheric observations and air-sea exchange models, Geophys. Res. Lett., 30, https://doi.org/10.1029/2003GL017933, 2003.

Singh, H. B., Salas, L. J., Chatfield, R. B., Czech, E., Fried, A., Walega, J., Evans, M. J., Field, B. D., Jacob, D. J., Blake, D., Heikes, B., Talbot, R., Sachse, G., Crawford, J. H., Avery, M. A., Sandholm, S., and Fuelberg, H.: Analysis of the atmospheric distribution, sources, and sinks of oxygenated volatile organic chemicals based on measurements over the Pacific during TRACE-P, J. Geophys. Res. Atmospheres, 109, https://doi.org/10.1029/2003JD003883, 2004.

Solberg, S., Dye, C., Schmidbauer, N., Herzog, A., and Gehrig, R.: Carbonyls and nonmethane hydrocarbons at rural European sites from the mediterranean to the arctic, J. Atmospheric Chem., 25, 33–66, https://doi.org/10.1007/BF00053285, 1996.

Thompson, C. R., Wofsy, S. C., Prather, M. J., Newman, P. A., Hanisco, T. F., Ryerson, T. B., Fahey, D. W., Apel, E. C., Brock, C. A., Brune, W. H., Froyd, K., Katich, J. M., Nicely, J. M., Peischl, J., Ray, E., Veres, P. R., Wang, S., Allen, H. M., Asher, E., Bian, H., Blake, D., Bourgeois, I., Budney, J., Bui, T. P., Butler, A., Campuzano-Jost, P., Chang, C., Chin, M., Commane, R., Correa, G., Crounse, J. D., Daube, B., Dibb, J. E., DiGangi, J. P., Diskin, G. S., Dollner, M., Elkins, J. W., Fiore, A. M., Flynn, C. M., Guo, H., Hall, S. R., Hannun, R. A., Hills, A., Hintsa, E. J., Hodzic, A., Hornbrook, R. S., Huey, L. G., Jimenez, J. L., Keeling, R. F., Kim, M. J., Kupc, A., Lacey, F., Lait, L. R., Lamarque, J.-F., Liu, J., McKain, K., Meinardi, S., Miller, D. O., Montzka, S. A., Moore, F. L., Morgan, E. J., Murphy, D. M., Murray, L. T., Nault, B. A., Neuman, J. A., Nguyen, L., Gonzalez, Y., Rollins, A., Rosenlof, K., Sargent, M., Schill, G., Schwarz, J. P., Clair, J. M. S., Steenrod, S. D., Stephens, B. B., Strahan, S. E., Strode, S. A., Sweeney, C., Thames, A. B., Ullmann, K., Wagner, N., Weber, R., Weinzierl, B., Wennberg, P. O., Williamson, C. J., Wolfe, G. M., and Zeng, L.: The NASA Atmospheric Tomography (ATom) Mission: Imaging the Chemistry of the Global Atmosphere, Bull. Am. Meteorol. Soc., 103, E761–E790, https://doi.org/10.1175/BAMS-D-20-0315.1, 2022.

Tsigaridis, K. and Kanakidou, M.: Global modelling of secondary organic aerosol in the troposphere: a sensitivity analysis, Atmos Chem Phys, 2003.

Wang, S., Apel, E. C., Schwantes, R. H., Bates, K. H., Jacob, D. J., Fischer, E. V., Hornbrook, R. S., Hills, A. J., Emmons, L. K., Pan, L. L., Honomichl, S., Tilmes, S., Lamarque, J.-F., Yang, M., Marandino, C. A., Saltzman, E. S., Bruyn, W. de, Kameyama, S., Tanimoto, H., Omori, Y., Hall, S. R., Ullmann, K., Ryerson, T. B., Thompson, C. R., Peischl, J., Daube, B. C., Commane, R., McKain, K., Sweeney, C., Thames, A. B., Miller, D. O., Brune, W. H., Diskin, G. S., DiGangi, J. P., and Wofsy, S. C.: Global Atmospheric Budget of Acetone: Air-Sea Exchange and the Contribution to Hydroxyl Radicals, J. Geophys. Res. Atmospheres, 125, e2020JD032553, https://doi.org/10.1029/2020JD032553, 2020.

Warneke, C. and de Gouw, J. A.: Organic trace gas composition of the marine boundary layer over the northwest Indian Ocean in April 2000, Atmos. Environ., 35, 5923–5933, https://doi.org/10.1016/S1352-2310(01)00384-3, 2001.

Weimer, M., Schröter, J., Eckstein, J., Deetz, K., Neumaier, M., Fischbeck, G., Hu, L., Millet, D. B., Rieger, D., Vogel, H., Vogel, B., Reddmann, T., Kirner, O., Ruhnke, R., and Braesicke, P.: An emission module for ICON-ART 2.0: implementation and simulations of acetone, Geosci. Model Dev., 10, 2471–2494, https://doi.org/10.5194/gmd-10-2471-2017, 2017.

Wesely, M. L. and Hicks, B. B.: Some Factors that Affect the Deposition Rates of Sulfur Dioxide and Similar Gases on Vegetation, J. Air Pollut. Control Assoc., 27, 1110–1116, https://doi.org/10.1080/00022470.1977.10470534, 1977.

Yoshino, A., Nakashima, Y., Miyazaki, K., Kato, S., Suthawaree, J., Shimo, N., Matsunaga, S., Chatani, S., Apel, E., Greenberg, J., Guenther, A., Ueno, H., Sasaki, H., Hoshi, J., Yokota, H., Ishii, K., and Kajii, Y.: Air quality diagnosis from comprehensive observations of total OH reactivity and reactive trace species in urban central Tokyo, Atmos. Environ., 49, 51–59, https://doi.org/10.1016/j.atmosenv.2011.12.029, 2012.

Yuan, B., Hu, W. W., Shao, M., Wang, M., Chen, W. T., Lu, S. H., Zeng, L. M., and Hu, M.: VOC emissions, evolutions and contributions to SOA formation at a receptor site in eastern China, Atmospheric Chem. Phys., 13, 8815–8832, https://doi.org/10.5194/acp-13-8815-2013, 2013.

Zhou, X. and Mopper, K.: Apparent partition coefficients of 15 carbonyl compounds between air and seawater and between air and freshwater; implications for air-sea exchange, Environ. Sci. Technol., 24, 1864–1869, https://doi.org/10.1021/es00082a013, 1990.

Supplementary Information For

Assessing acetone for the GISS ModelE2.1 Earth system model

Alexandra Rivera[1], Kostas Tsigaridis[2,3], Gregory Faluvegi[2,3], Drew Shindell[4]

[1]Pratt School of Engineering, Duke University, Durham, NC, 27708, USA
[2]Center for Climate Systems Research, Columbia University, 2880 Broadway, New York, NY, 10025, USA
[3]NASA Goddard Institute for Space Studies, 2880 Broadway, New York, NY, 10025, USA
[4]Nicholas School of the Environment, Duke University, Durham, NC, 27708, USA

Correspondence to: Kostas Tsigaridis (kostas.tsigaridis@columbia.edu)

2.3.1 Chemical sources

The acetone molar yields of propane, butane, pentane, and higher alkanes were derived with suggestions from the literature (Fischbeck et al., 2017; Jacob et al., 2002; Weimer et al., 2017). We used a molar yield of 0.73 for propane, derived by averaging 0.72 from Jacob et al. (2002) and 0.736 from Weimer et al. (2017). Our molar yield of 0.95 for butane was derived by averaging 0.96 from Fischbeck et al. (2017) and 0.93 from Jacob et al. (2002). Our molar yield of 0.63 for pentane was derived by averaging 0.72 from Fischbeck et al. (2017) and 0.53 from Jacob et al. (2002). Finally, we used a molar yield of 0.79 for higher alkanes, derived from averaging the following four values: 0.96 for isobutane and 0.72 for isopentane in Fischbeck et al. (2017), and 0.93 for isobutane and 0.53 for isopentane in Jacob et al. (2002).

3.1 Global acetone budget and burden

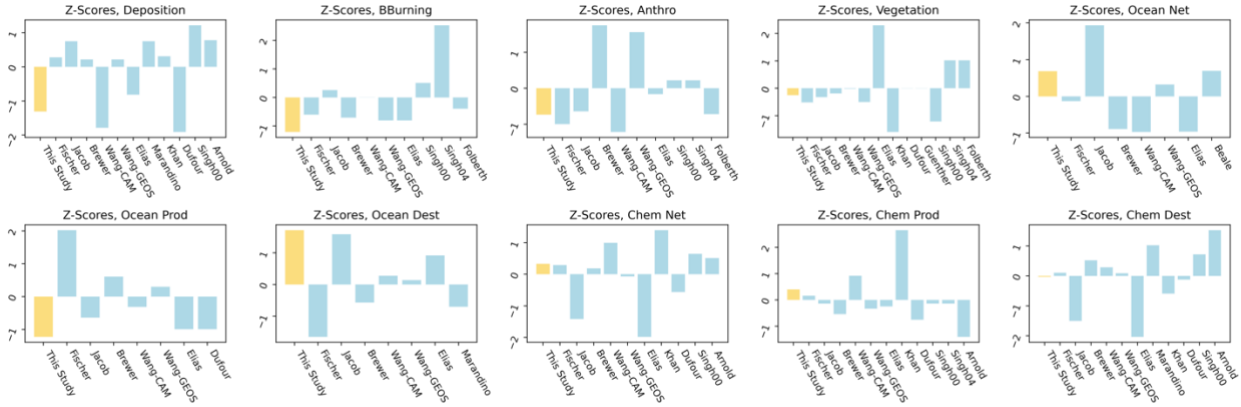

Figure S1. The data recorded in the literature was used to determine a mean for each budget flux value, and the distance from that mean for each paper was expressed as a z-score (Arnold et al., 2005; Beale et al., 2013; Brewer et al., 2017; Dufour et al., 2016; Elias et al., 2011; Fischer et al., 2012; Folberth et al., 2006; Guenther et al., 2012; Jacob et al., 2002; Khan et al., 2015; Marandino et al., 2005; Singh et al., 2000, 2004; Wang et al., 2020).The z-scores for the literature are in shown as light-blue bars, and the Baseline model's z-score is highlighted in yellow.

3.2 Spatial distribution of acetone

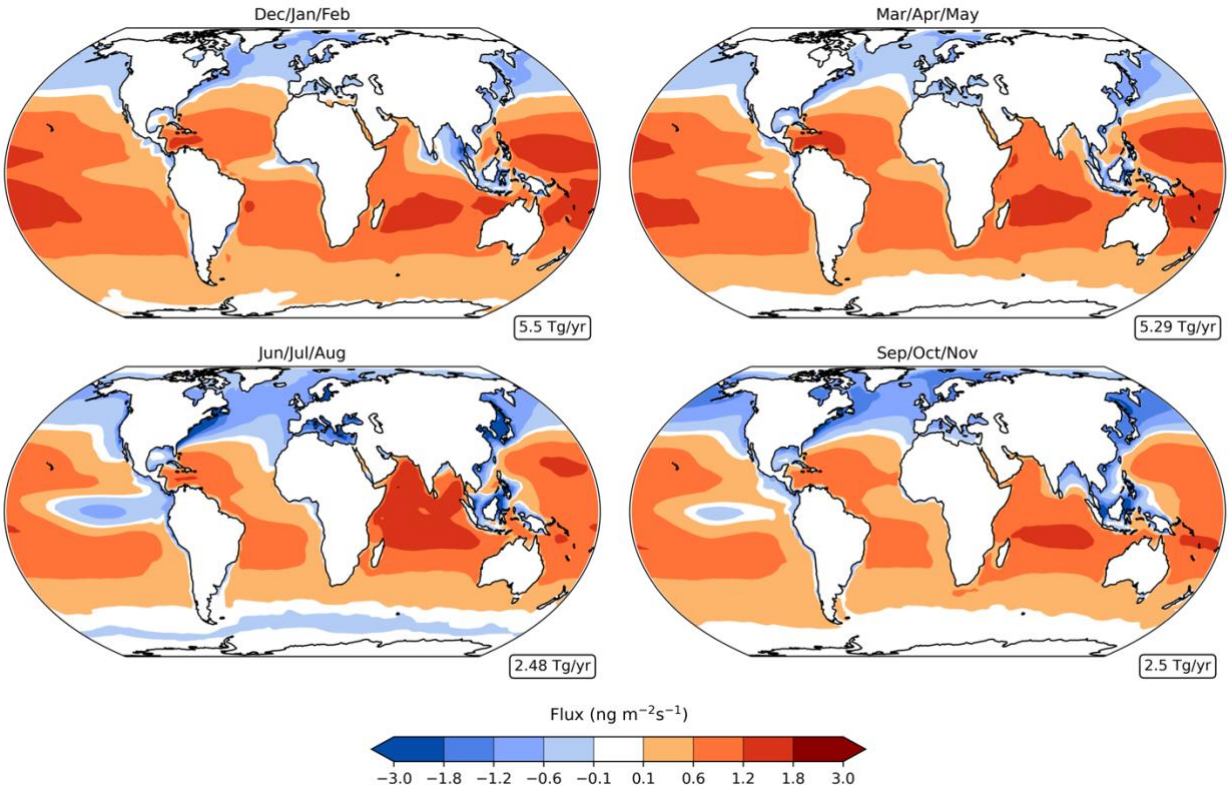

Figure S2. Net oceanic acetone fluxes in the Baseline simulation for December-February (top left), March-May (top right), June-August (bottom left), and September-November (bottom right), with red indicating a net source and blue indicating a net sink. Nonlinear colorbars are used to better differentiate the details in the map. The weighted global means of the net ocean fluxes are shown in boxes on the lower right.

3.3 Vertical distribution of acetone

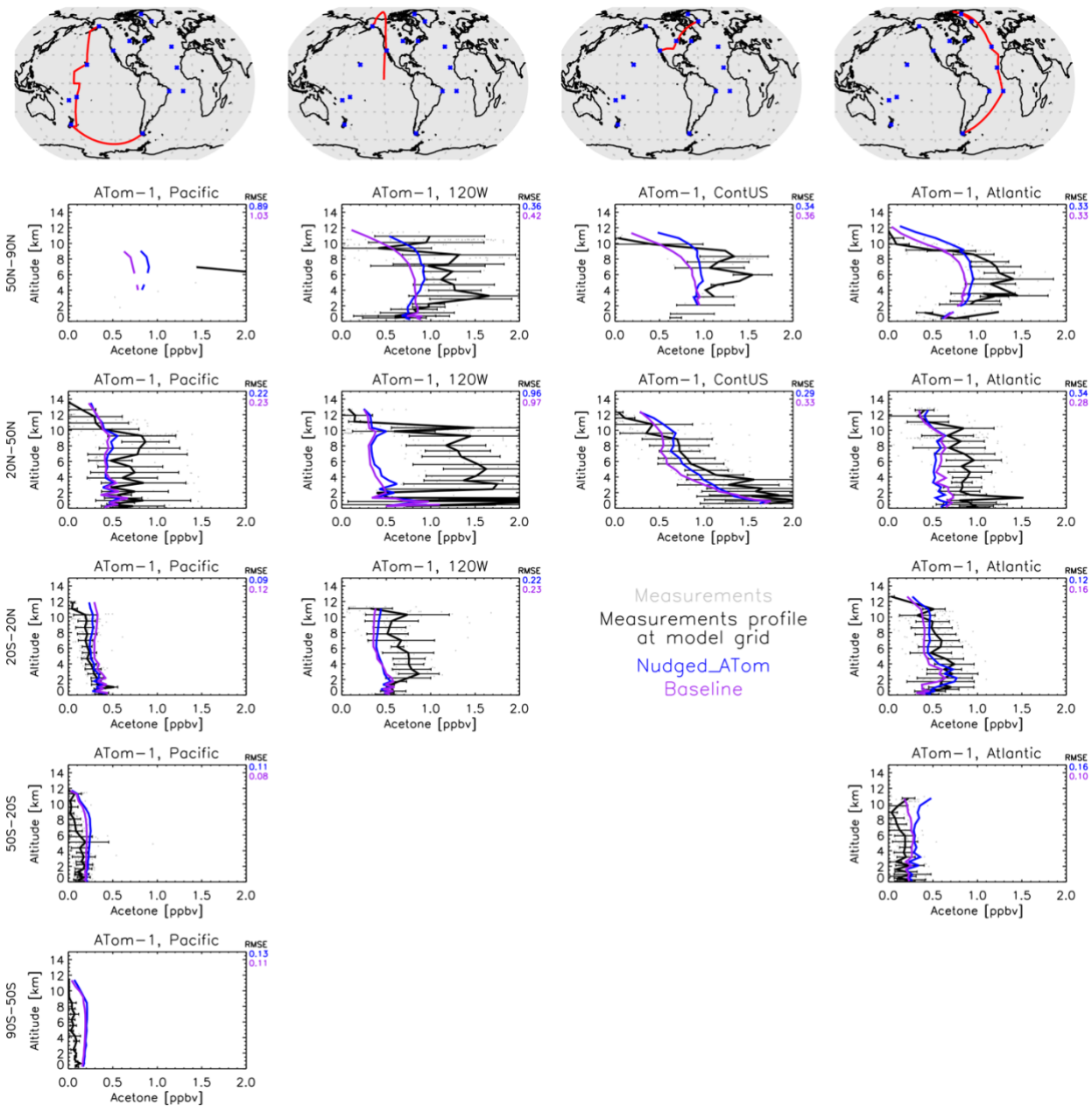

Figure S3. Comparison between the GISS ModelE2.1 simulations (Baseline in purple and Nudged_ATom in blue) and the ATom-1 field measurements (July-August 2016). Individual data points are shown with grey dots, and their average values are shown in black, with error bars representing the one-sigma range of the averages. The root mean square error (RMSE) of each simulation is shown at the top right of each plot.

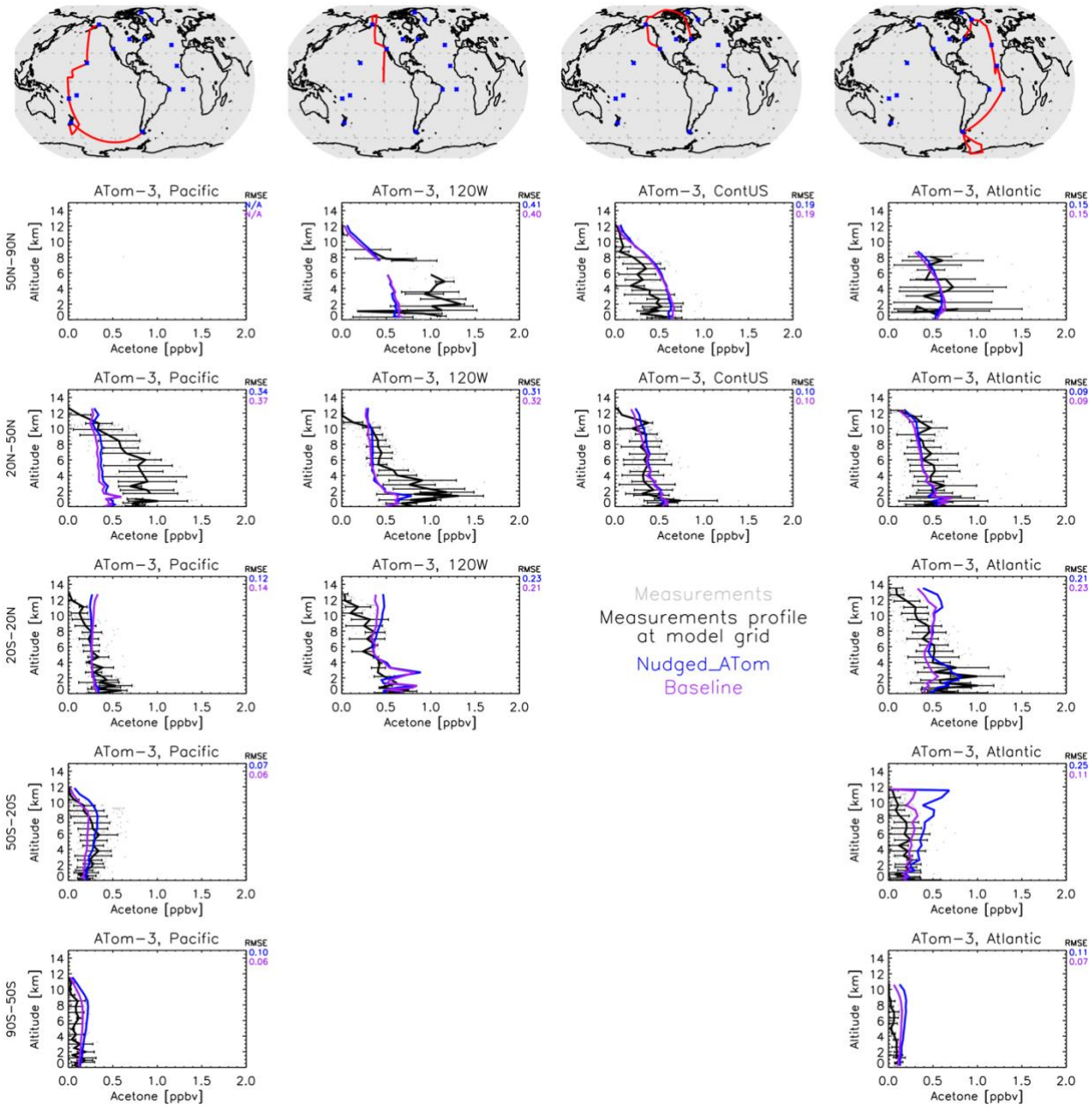

Figure S4. Similar to Figure S3, except for the ATom-3 field measurements (September-October 2017).

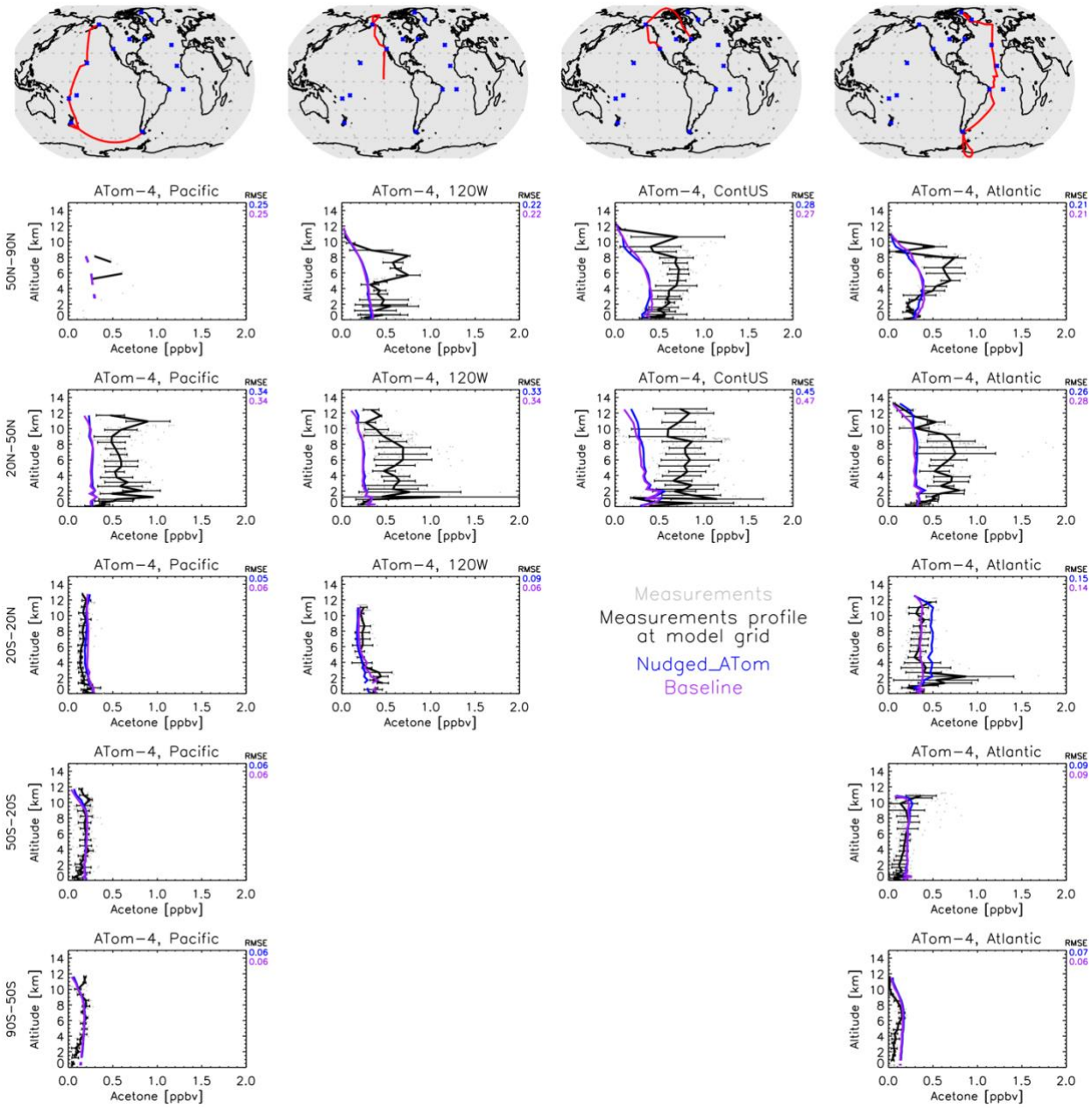

Figure S5. Similar to Figure S3, except for the ATom-4 field measurements (April-May 2018).

3.4 Seasonality of acetone

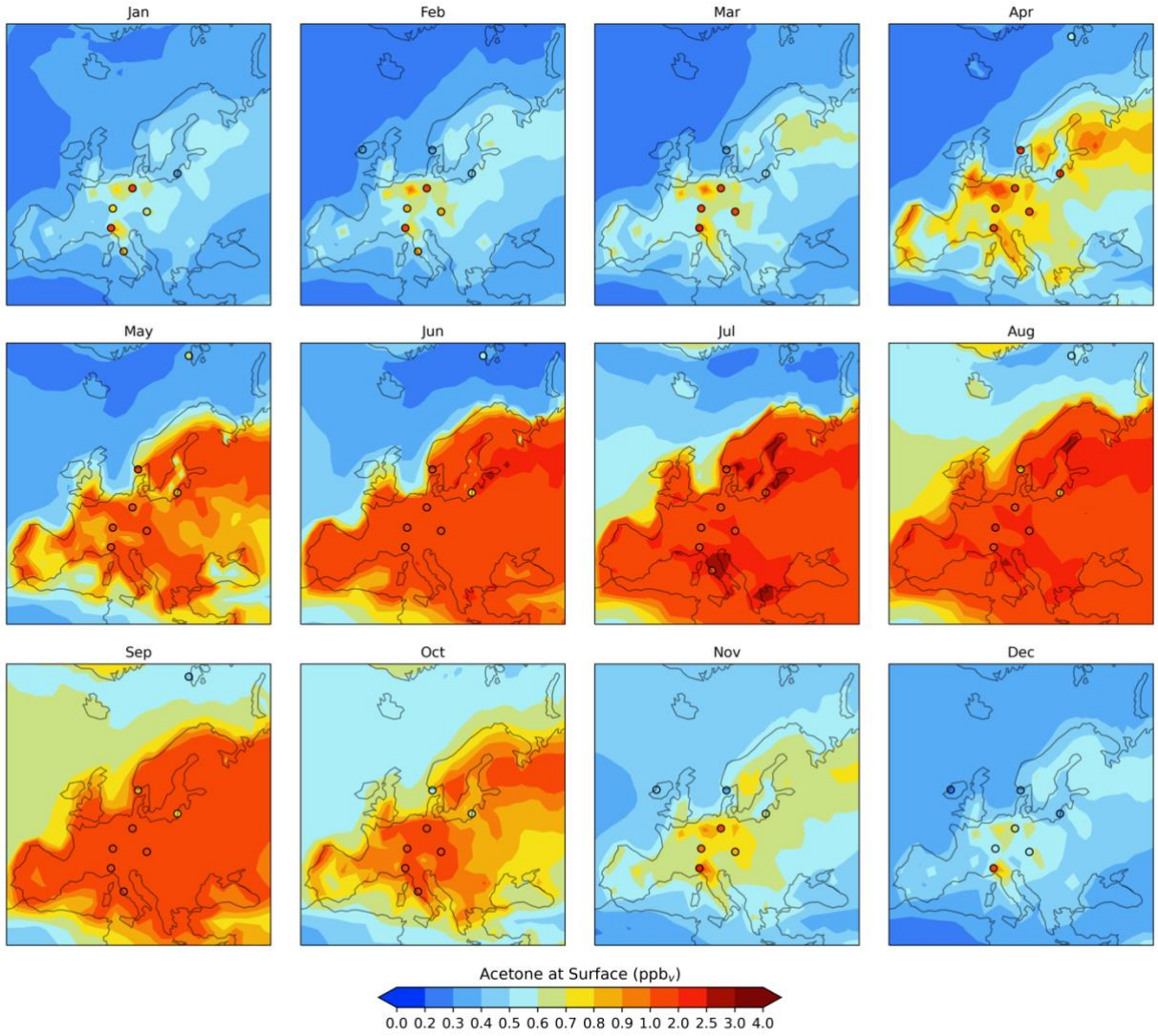

Figure S6. GISS ModelE2.1 spatial distribution of annual mean acetone at surface for the Baseline simulation in Europe over twelve months. Filled circles represent data from field measurements from Solberg et al. (1996). A nonlinear colorbar is used to better differentiate the details in the map.

3.5 Sensitivity Studies

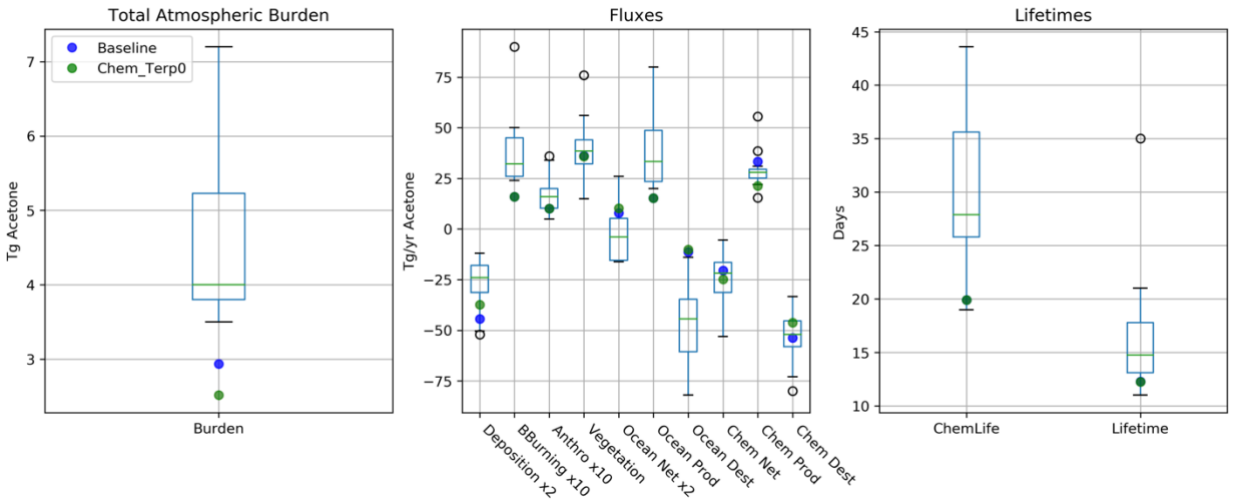

Figure S7. Total atmospheric burden, fluxes, and lifetimes of acetone from the literature (shown in boxes and whiskers with outliers as open circles) (Arnold et al., 2005; Beale et al., 2013; Brewer et al., 2017; Dufour et al., 2016; Elias et al., 2011; Fischer et al., 2012; Folberth et al., 2006; Guenther et al., 2012; Jacob et al., 2002; Khan et al., 2015; Marandino et al., 2005; Singh et al., 2000, 2004; Wang et al., 2020), values from GISS ModelE2.1 Baseline simulation (solid blue circles), and values from the Chem_Terp0 sensitivity study (green circles).

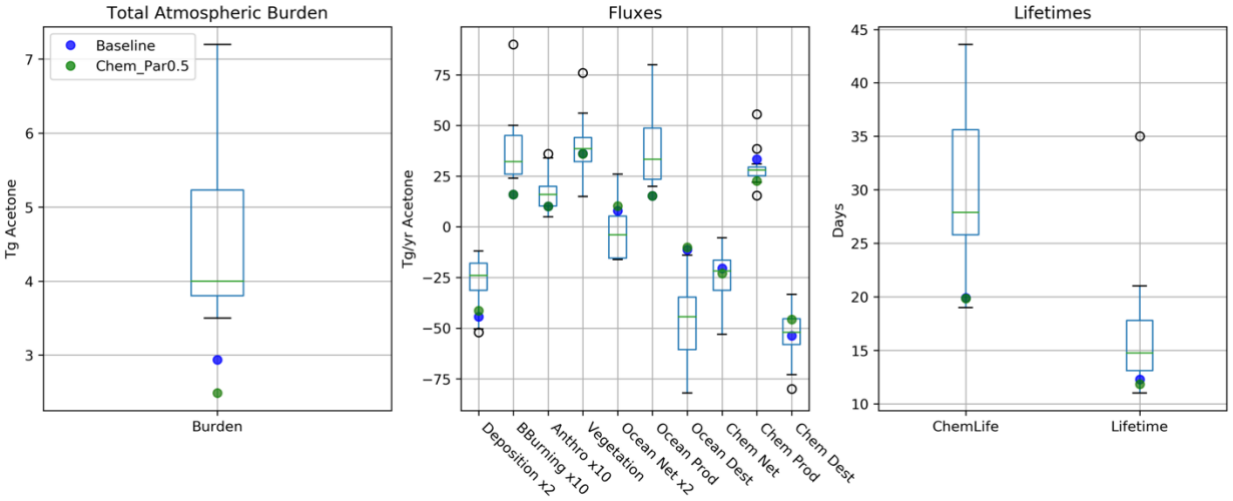

Figure S8. Similar to Figure S7, except values from the Chem_Par0.5 sensitivity study as green circles.

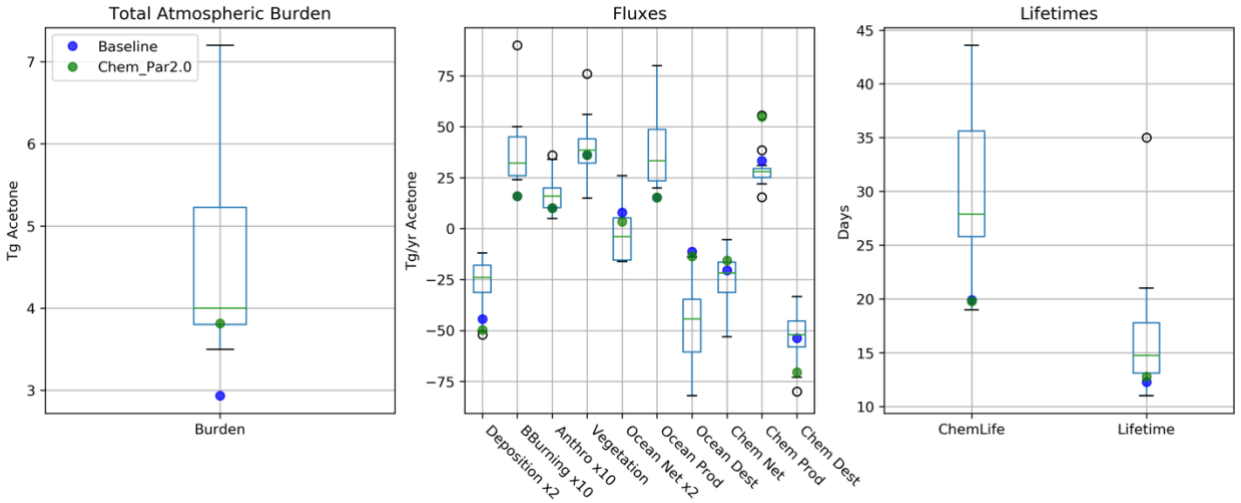

62

63 **Figure S9.** Similar to Figure S7, except values from the Chem_Par2.0 sensitivity study as green circles.

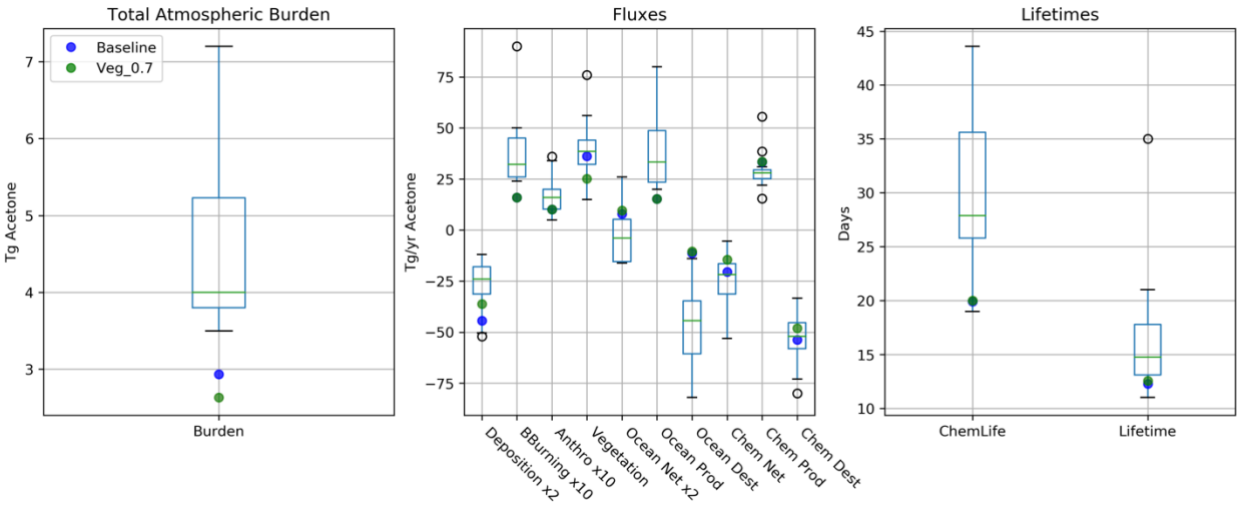

64

65 **Figure S10.** Similar to Figure S7, except values from the Veg_0.7 sensitivity study as green circles.

66

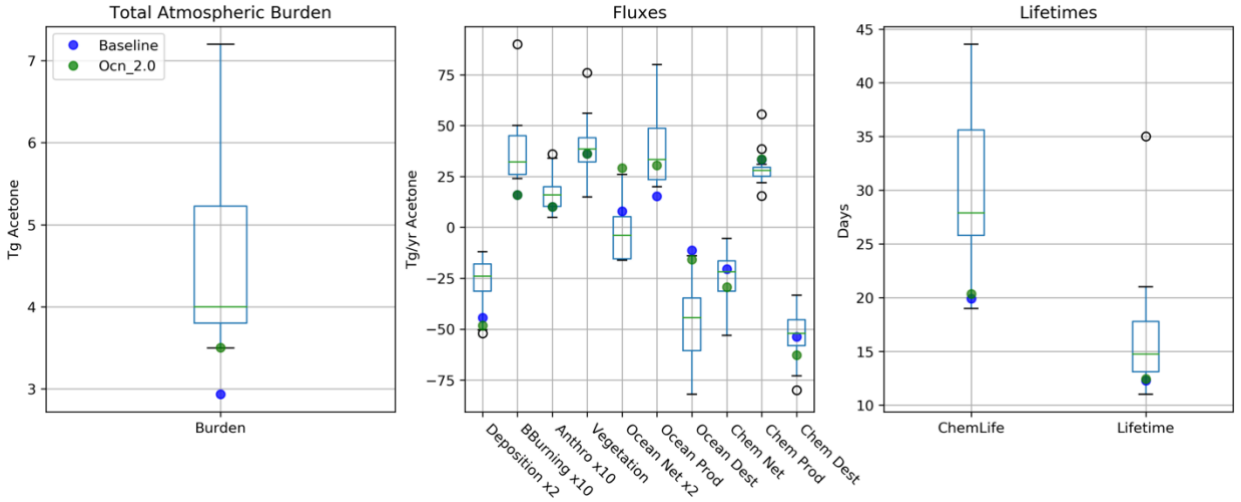

67

68 **Figure S11.** Similar to Figure S7, except values from the Ocn_2.0 sensitivity study as green circles.

69

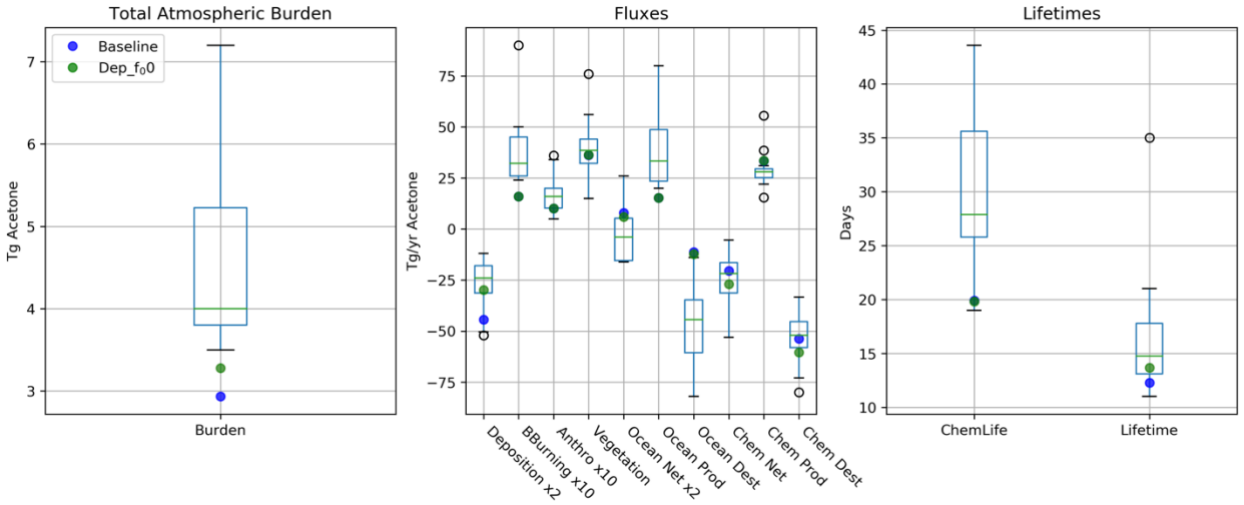

Figure S12. Similar to Figure S7, except values from the Dep_f$_0$0 sensitivity study as green circles.

3.5.1 Chemistry

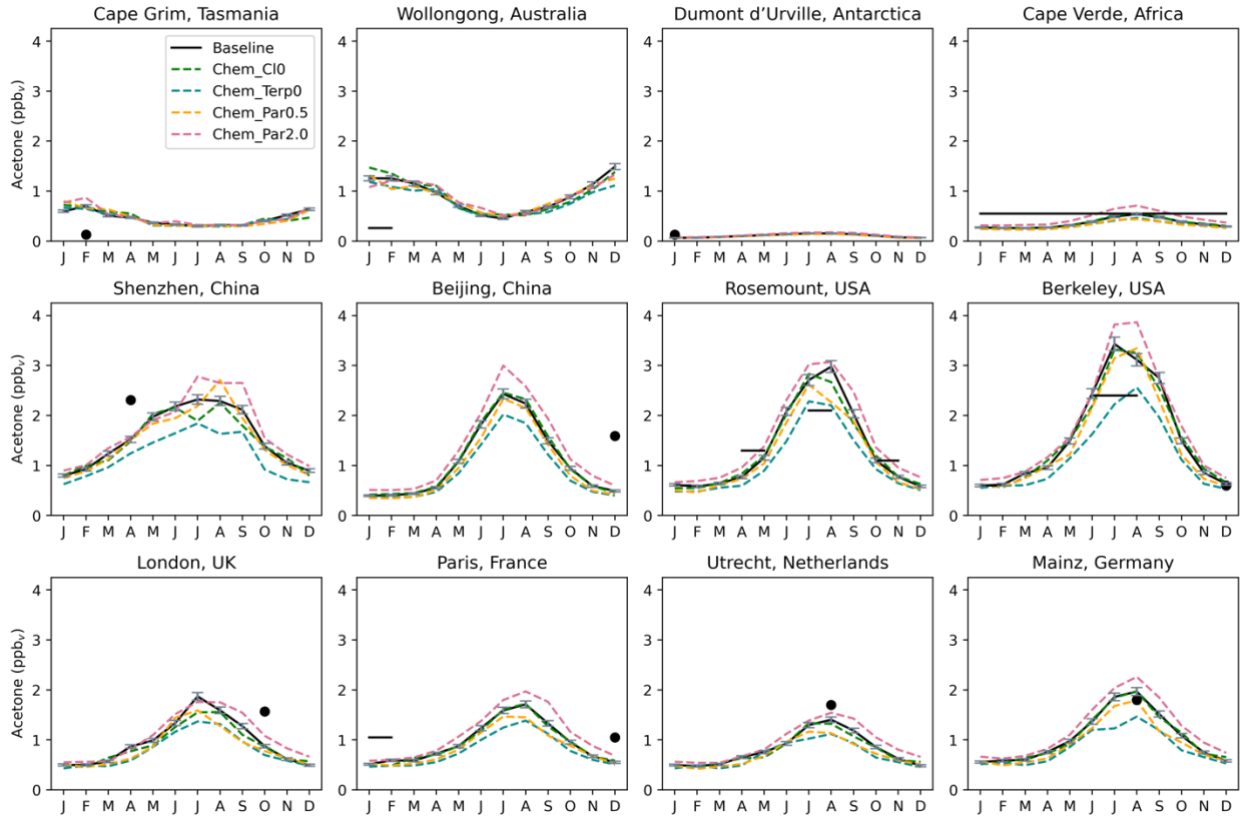

Figure S13. Acetone over twelve months for various sites that do not have enough measurements to resolve seasonality (Australia, Antarctica, Africa, Asia, Europe, North America). The modelled estimates of acetone at the surface from the Baseline simulation are shown as solid black lines, and the sensitivity studies are as follows: removing the acetone + chlorine reaction (dashed green lines), removing the production of acetone from terpenes (dashed blue lines), halving the yield of acetone from paraffin (dashed orange lines), and doubling the yield of acetone from paraffin (dashed pink lines). The modelled estimates are overlaid with monthly (solid circles) or seasonal (solid lines) field measurements, as found in the literature (de Gouw et al.,

2004; Dolgorouky et al., 2012; Galbally et al., 2007; Guérette et al., 2019; Hu et al., 2013; Huang et al., 2020; Langford et al., 2010; Legrand et al., 2012; Li et al., 2019; Read et al., 2012; Schade and Goldstein, 2006).

3.5.2 Terrestrial and oceanic fluxes

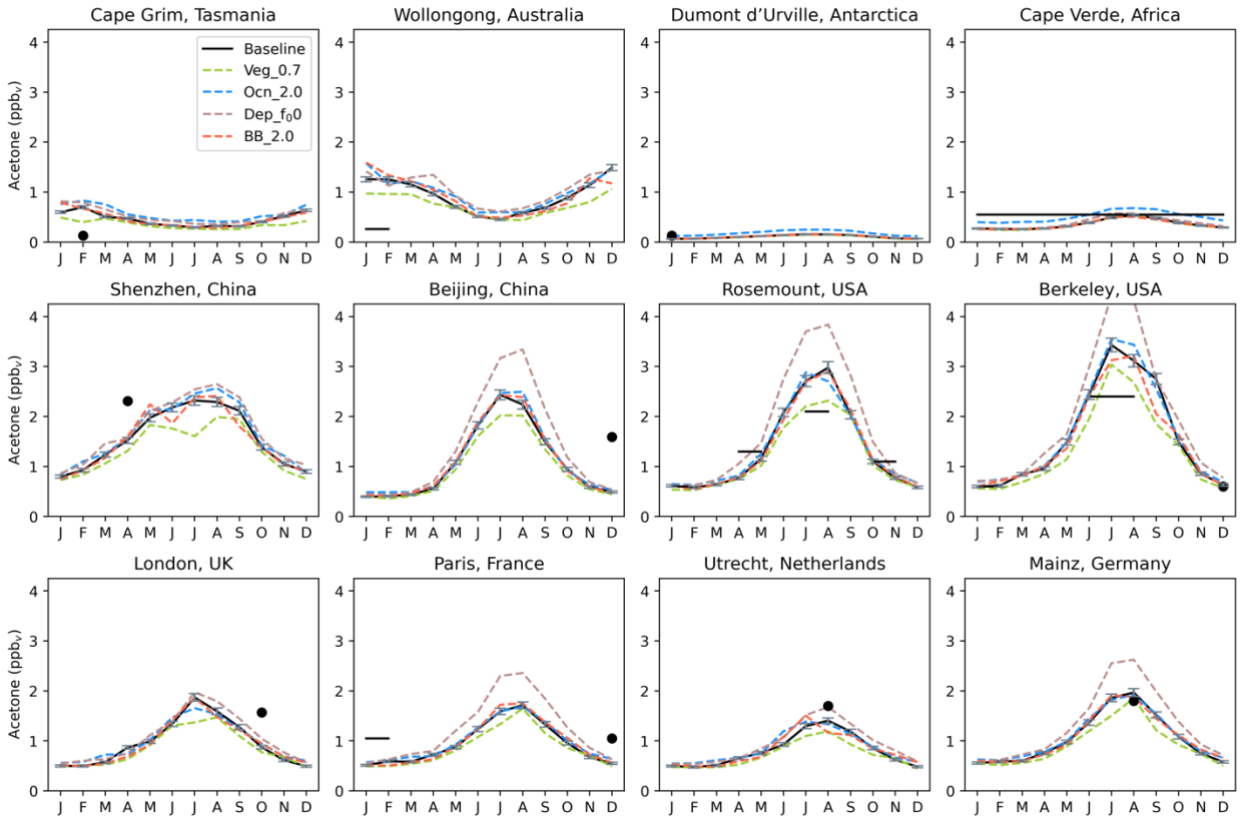

Figure S14. Similar to Figure S13, but with the terrestrial and oceanic sensitivity studies added. The modelled estimates of acetone at the surface from the Baseline simulation are shown as solid black lines, and the sensitivity studies are as follows: reducing vegetation emissions to 0.7 acetone from MEGAN (dashed light-green line), doubling ocean acetone concentration (dashed blue line), changing the reactivity factor for dry deposition (dashed brown line), and doubling biomass burning emissions (dashed orange line). Field measurements from Solberg et al., (1996) are shown as solid black dots. The modelled estimates are overlaid with monthly (solid circles) or seasonal (solid lines) field measurements, as found in the literature (de Gouw et al., 2004; Dolgorouky et al., 2012; Galbally et al., 2007; Guérette et al., 2019; Hu et al., 2013; Huang et al., 2020; Langford et al., 2010; Legrand et al., 2012; Li et al., 2019; Read et al., 2012; Schade and Goldstein, 2006).

3.5.3 ATom comparisons

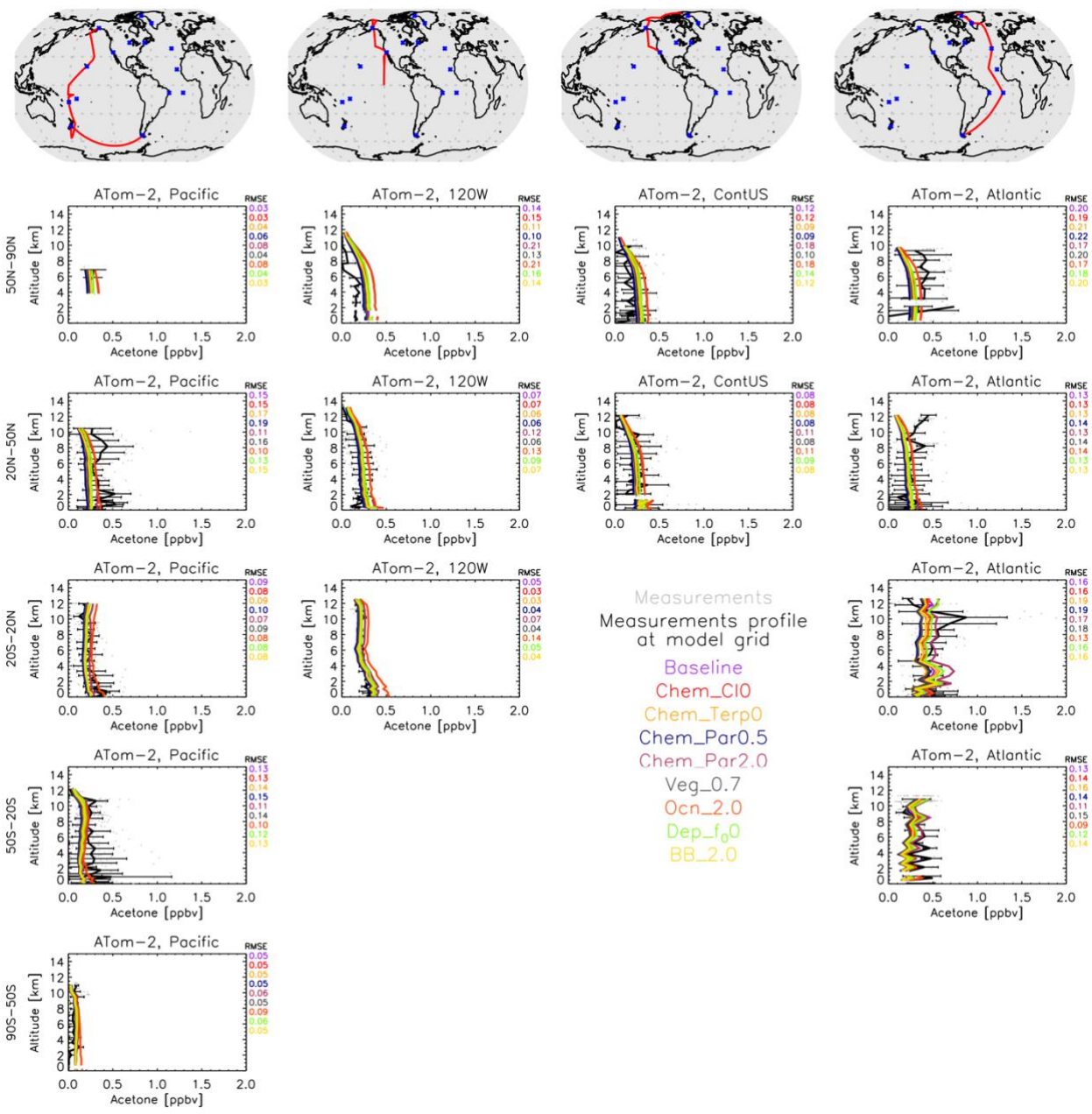

Figure S15. Similar to Figure S3, except a comparison between the GISS ModelE2.1 sensitivity simulations and the ATom-2 aircraft measurements (January-February 2017). Individual data points are shown with grey dots, and their average values are shown in black, with error bars representing the one-sigma range of the averages. The root mean square error (RMSE) of each simulation is shown at the top right of each plot. Note that all sensitivities are to be compared against the Baseline simulation.

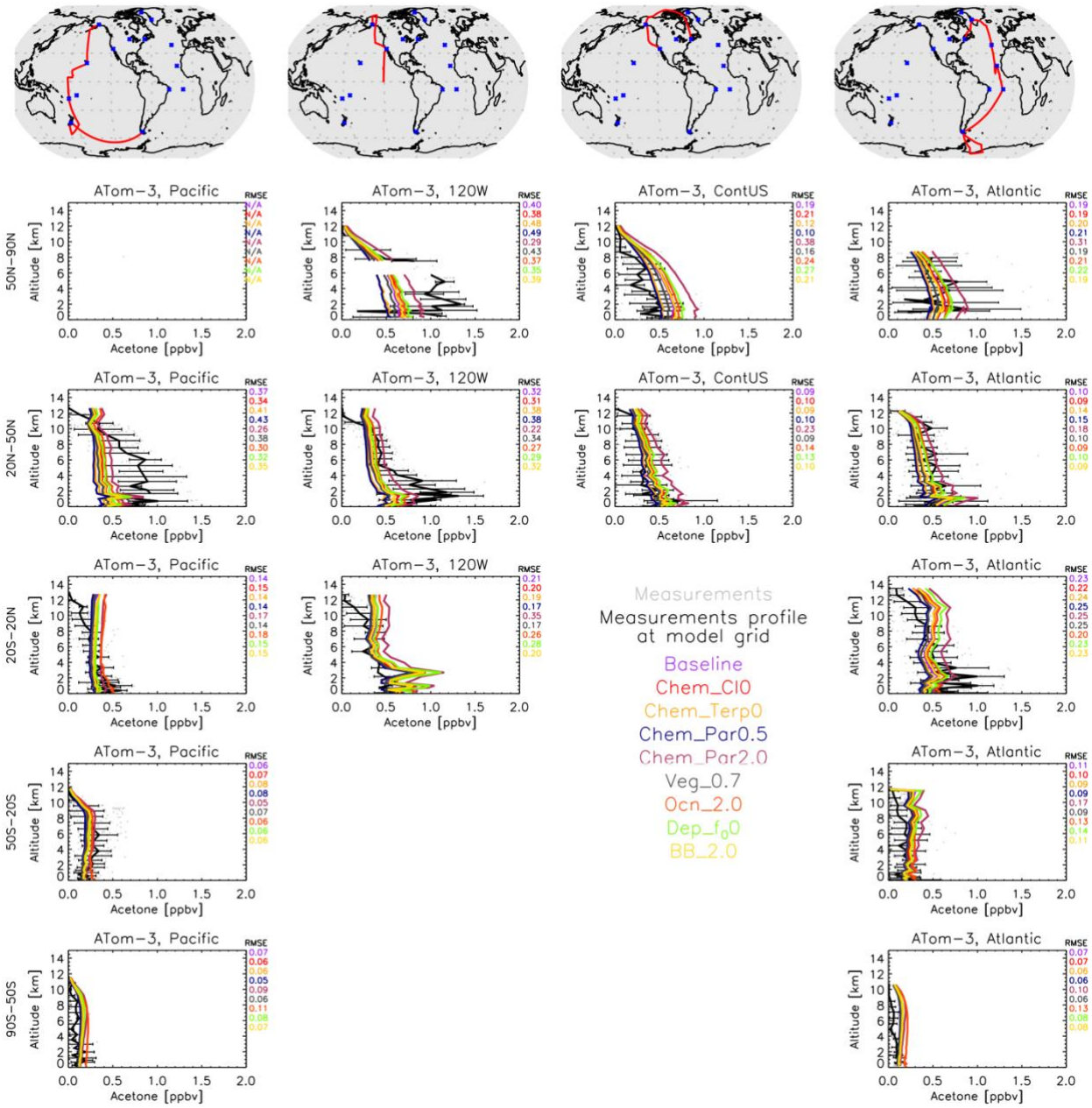

Figure S16. Similar to Figure S15, except for the ATom-3 field measurements (September-October 2017).

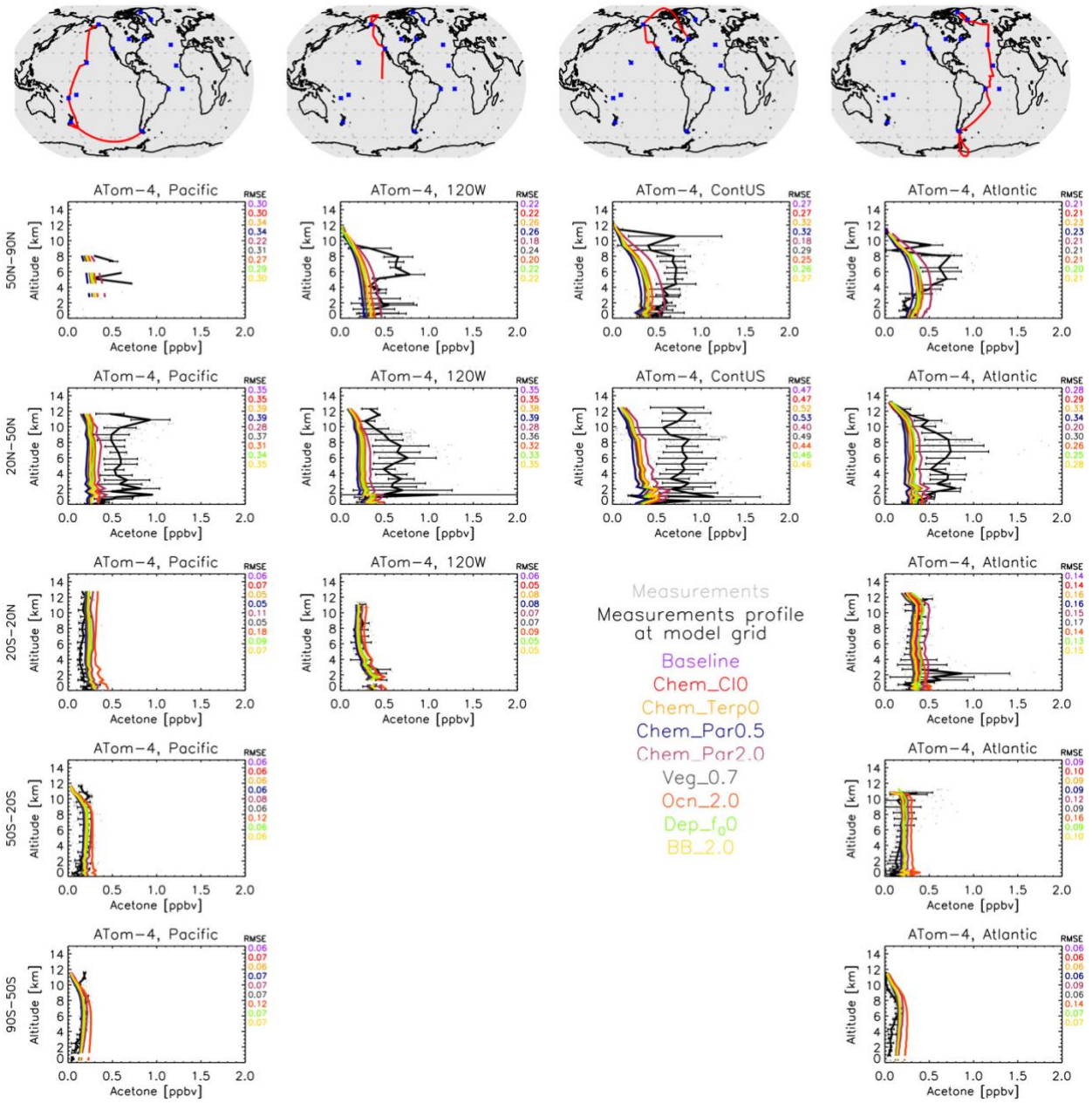

Figure S17. Similar to Figure S15, except for the ATom-4 field measurements (April-May 2018).

References

Arnold, S. R., Chipperfield, M. P., and Blitz, M. A.: A three-dimensional model study of the effect of new temperature-dependent quantum yields for acetone photolysis, J. Geophys. Res. Atmospheres, 110, https://doi.org/10.1029/2005JD005998, 2005.

Beale, R., Dixon, J. L., Arnold, S. R., Liss, P. S., and Nightingale, P. D.: Methanol, acetaldehyde, and acetone in the surface waters of the Atlantic Ocean, J. Geophys. Res. Oceans, 118, 5412–5425, https://doi.org/10.1002/jgrc.20322, 2013.

Brewer, J. F., Bishop, M., Kelp, M., Keller, C. A., Ravishankara, A. R., and Fischer, E. V.: A sensitivity analysis of key natural factors in the modeled global acetone budget, J. Geophys. Res. Atmospheres, 122, 2043–2058, https://doi.org/10.1002/2016JD025935, 2017.

Dolgorouky, C., Gros, V., Sarda-Esteve, R., Sinha, V., Williams, J., Marchand, N., Sauvage, S., Poulain, L., Sciare, J., and Bonsang, B.: Total OH reactivity measurements in Paris during the 2010 MEGAPOLI winter campaign, Atmospheric Chem. Phys., 12, 9593–9612, https://doi.org/10.5194/acp-12-9593-2012, 2012.

Dufour, G., Szopa, S., Harrison, J. J., Boone, C. D., and Bernath, P. F.: Seasonal variations of acetone in the upper troposphere–lower stratosphere of the northern midlatitudes as observed by ACE-FTS, J. Mol. Spectrosc., 323, 67–77, https://doi.org/10.1016/j.jms.2016.02.006, 2016.

Elias, T., Szopa, S., Zahn, A., Schuck, T., Brenninkmeijer, C., Sprung, D., and Slemr, F.: Acetone variability in the upper troposphere: analysis of CARIBIC observations and LMDz-INCA chemistry-climate model simulations, Atmospheric Chem. Phys., 11, 8053–8074, https://doi.org/10.5194/acp-11-8053-2011, 2011.

Fischbeck, G., Bönisch, H., Neumaier, M., Brenninkmeijer, C. A. M., Orphal, J., Brito, J., Becker, J., Sprung, D., van Velthoven, P. F. J., and Zahn, A.: Acetone–CO enhancement ratios in the upper troposphere based on 7 years of CARIBIC data: new insights and estimates of regional acetone fluxes, Atmospheric Chem. Phys., 17, 1985–2008, https://doi.org/10.5194/acp-17-1985-2017, 2017.

Fischer, E. V., Jacob, D. J., Millet, D. B., Yantosca, R. M., and Mao, J.: The role of the ocean in the global atmospheric budget of acetone, Geophys. Res. Lett., 39, https://doi.org/10.1029/2011GL050086, 2012.

Folberth, G. A., Hauglustaine, D. A., Lathière, J., and Brocheton, F.: Interactive chemistry in the Laboratoire de Météorologie Dynamique general circulation model: model description and impact analysis of biogenic hydrocarbons on tropospheric chemistry, Atmospheric Chem. Phys., 6, 2273–2319, https://doi.org/10.5194/acp-6-2273-2006, 2006.

Galbally, I., Lawson, S. J., Bentley, S., Gillett, R., Meyer, M., and Goldstein, A.: Volatile organic compounds in marine air at Cape Grim, Australia, Environ. Chem. - Env. CHEM, 4, https://doi.org/10.1071/EN07024, 2007.

de Gouw, J., Warneke, C., Holzinger, R., Klüpfel, T., and Williams, J.: Inter-comparison between airborne measurements of methanol, acetonitrile and acetone using two differently configured PTR-MS instruments, Int. J. Mass Spectrom., 239, 129–137, https://doi.org/10.1016/j.ijms.2004.07.025, 2004.

Guenther, A. B., Jiang, X., Heald, C. L., Sakulyanontvittaya, T., Duhl, T., Emmons, L. K., and Wang, X.: The Model of Emissions of Gases and Aerosols from Nature version 2.1 (MEGAN2.1): an extended and updated framework for modeling biogenic emissions, Geosci. Model Dev., 5, 1471–1492, https://doi.org/10.5194/gmd-5-1471-2012, 2012.

Guérette, É.-A., Paton-Walsh, C., Galbally, I., Molloy, S., Lawson, S., Kubistin, D., Buchholz, R., Griffith, D. W. T., Langenfelds, R. L., Krummel, P. B., Loh, Z., Chambers, S., Griffiths, A., Keywood, M., Selleck, P., Dominick, D., Humphries, R., and Wilson, S. R.: Composition of Clean Marine Air and Biogenic Influences on VOCs during the MUMBA Campaign, Atmosphere, 10, 383, https://doi.org/10.3390/atmos10070383, 2019.

Hu, L., Millet, D. B., Kim, S. Y., Wells, K. C., Griffis, T. J., Fischer, E. V., Helmig, D., Hueber, J., and Curtis, A. J.: North American acetone sources determined from tall tower measurements and inverse modeling, Atmospheric Chem. Phys., 13, 3379–3392, https://doi.org/10.5194/acp-13-3379-2013, 2013.

Huang, X.-F., Zhang, B., Xia, S.-Y., Han, Y., Wang, C., Yu, G.-H., and Feng, N.: Sources of oxygenated volatile organic compounds (OVOCs) in urban atmospheres in North and South China, Environ. Pollut., 261, 114152, https://doi.org/10.1016/j.envpol.2020.114152, 2020.

Jacob, D. J., Field, B. D., Jin, E. M., Bey, I., Li, Q., Logan, J. A., Yantosca, R. M., and Singh, H. B.: Atmospheric budget of acetone, J. Geophys. Res. Atmospheres, 107, ACH 5-1-ACH 5-17, https://doi.org/10.1029/2001JD000694, 2002.

Khan, M. A. H., Cooke, M. C., Utembe, S. R., Archibald, A. T., Maxwell, P., Morris, W. C., Xiao, P., Derwent, R. G., Jenkin, M. E., Percival, C. J., Walsh, R. C., Young, T. D. S., Simmonds, P. G., Nickless, G., O'Doherty, S., and Shallcross, D. E.: A study of global atmospheric budget and distribution of acetone using global atmospheric model STOCHEM-CRI, Atmos. Environ., 112, 269–277, https://doi.org/10.1016/j.atmosenv.2015.04.056, 2015.

Langford, B., Nemitz, E., House, E., Phillips, G. J., Famulari, D., Davison, B., Hopkins, J. R., Lewis, A. C., and Hewitt, C. N.: Fluxes and concentrations of volatile organic compounds above central London, UK, Atmospheric Chem. Phys., 10, 627–645, https://doi.org/10.5194/acp-10-627-2010, 2010.

Legrand, M., Gros, V., Preunkert, S., Sarda-Estève, R., Thierry, A.-M., Pépy, G., and Jourdain, B.: A reassessment of the budget of formic and acetic acids in the boundary layer at Dumont d'Urville (coastal Antarctica): The role of penguin emissions on the budget of several oxygenated volatile organic compounds, J. Geophys. Res. Atmospheres, 117, https://doi.org/10.1029/2011JD017102, 2012.

Li, K., Li, J., Tong, S., Wang, W., Huang, R.-J., and Ge, M.: Characteristics of wintertime VOCs in suburban and urban Beijing: concentrations, emission ratios, and festival effects, Atmospheric Chem. Phys., 19, 8021–8036, https://doi.org/10.5194/acp-19-8021-2019, 2019.

Marandino, C. A., Bruyn, W. J. D., Miller, S. D., Prather, M. J., and Saltzman, E. S.: Oceanic uptake and the global atmospheric acetone budget, Geophys. Res. Lett., 32, https://doi.org/10.1029/2005GL023285, 2005.

Read, K. A., Carpenter, L. J., Arnold, S. R., Beale, R., Nightingale, P. D., Hopkins, J. R., Lewis, A. C., Lee, J. D., Mendes, L., and Pickering, S. J.: Multiannual Observations of Acetone, Methanol, and Acetaldehyde in Remote Tropical Atlantic Air: Implications for Atmospheric OVOC Budgets and Oxidative Capacity, Environ. Sci. Technol., 46, 11028–11039, https://doi.org/10.1021/es302082p, 2012.

Schade, G. W. and Goldstein, A. H.: Seasonal measurements of acetone and methanol: Abundances and implications for atmospheric budgets, Glob. Biogeochem. Cycles, 20, https://doi.org/10.1029/2005GB002566, 2006.

Singh, H., Chen, Y., Tabazadeh, A., Fukui, Y., Bey, I., Yantosca, R., Jacob, D., Arnold, F., Wohlfrom, K., Atlas, E., Flocke, F., Blake, D., Blake, N., Heikes, B., Snow, J., Talbot, R., Gregory, G., Sachse, G., Vay, S., and Kondo, Y.: Distribution and fate of selected oxygenated organic species in the troposphere and lower stratosphere over the Atlantic, J. Geophys. Res. Atmospheres, 105, 3795–3805, https://doi.org/10.1029/1999JD900779, 2000.

Singh, H. B., Salas, L. J., Chatfield, R. B., Czech, E., Fried, A., Walega, J., Evans, M. J., Field, B. D., Jacob, D. J., Blake, D., Heikes, B., Talbot, R., Sachse, G., Crawford, J. H., Avery, M. A., Sandholm, S., and Fuelberg, H.: Analysis of the atmospheric distribution, sources, and sinks of oxygenated volatile organic chemicals based on measurements over the Pacific during TRACE-P, J. Geophys. Res. Atmospheres, 109, https://doi.org/10.1029/2003JD003883, 2004.

Solberg, S., Dye, C., Schmidbauer, N., Herzog, A., and Gehrig, R.: Carbonyls and nonmethane hydrocarbons at rural European sites from the mediterranean to the arctic, J. Atmospheric Chem., 25, 33–66, https://doi.org/10.1007/BF00053285, 1996.

Wang, S., Apel, E. C., Schwantes, R. H., Bates, K. H., Jacob, D. J., Fischer, E. V., Hornbrook, R. S., Hills, A. J., Emmons, L. K., Pan, L. L., Honomichl, S., Tilmes, S., Lamarque, J.-F., Yang, M., Marandino, C. A., Saltzman, E. S., Bruyn, W. de, Kameyama, S., Tanimoto, H., Omori, Y., Hall, S. R., Ullmann, K., Ryerson, T. B., Thompson, C. R., Peischl, J., Daube, B. C., Commane, R., McKain, K., Sweeney, C., Thames, A. B., Miller, D. O., Brune, W. H., Diskin, G. S., DiGangi, J. P., and Wofsy, S. C.: Global Atmospheric Budget of Acetone: Air-Sea Exchange and the Contribution to Hydroxyl Radicals, J. Geophys. Res. Atmospheres, 125, e2020JD032553, https://doi.org/10.1029/2020JD032553, 2020.

Weimer, M., Schröter, J., Eckstein, J., Deetz, K., Neumaier, M., Fischbeck, G., Hu, L., Millet, D. B., Rieger, D., Vogel, H., Vogel, B., Reddmann, T., Kirner, O., Ruhnke, R., and Braesicke, P.: An emission module for ICON-ART 2.0: implementation and simulations of acetone, Geosci. Model Dev., 10, 2471–2494, https://doi.org/10.5194/gmd-10-2471-2017, 2017.